# Charge crossover at the U(1) Higgs phase transition

Article (Published Version)

# Charge crossover at the $U(1)$-Higgs phase transition

Filipe Freire*
*Department of Mathematical Physics, National University of Ireland, Maynooth, Ireland*
*and School of Theoretical Physics, Dublin Institute for Advanced Studies, 10 Burlington Road,*
*Dublin 4, Ireland*

Daniel F. Litim†
*Institut für Theoretische Physik, Philosophenweg 16, D-69120 Heidelberg, Germany*
(Received 22 February 2000; published 27 July 2001)

The type-I region of phase transitions at finite temperature of the $U(1)$-Higgs theory in $3+1$ dimensions is investigated in detail using a Wilsonian renormalization group. We consider, in particular, the quantitative effects induced through the crossover of the scale-dependent Abelian charge from the Gaussian to a nontrivial Abelian fixed point. As a result, the strength of the first-order phase transition is weakened. Analytical solutions to approximate flow equations are obtained, and all characteristics of the phase transition are discussed and compared to the results obtained from perturbation theory. In addition, we present a detailed quantitative study regarding the dependence of the physical observables on the coarse-graining scheme. This results in error bars for the regularization scheme (RS) dependence. We find quantitative evidence for an intimate link between the RS dependence and truncations of flow equations.

DOI: 10.1103/PhysRevD.64.045014 PACS number(s): 11.10.Wx, 05.70.Fh, 11.10.Hi, 11.15.Tk

## I. INTRODUCTION

The phase transition of the $U(1)$-Higgs theory in $3+1$ dimensions at finite temperature provides an important model for cosmological phase transitions. In the high-temperature limit, it reduces to the purely three-dimensional (3D) Abelian Higgs model describing the superconducting phase transition [1], or certain nematic to smectic-$A$ phase transitions in liquid crystals [2]. The phase transition in this model is governed by the infrared region of its spectrum of fluctuations. The nature of the phase transition depends primarily on the ratio $m_H/m_A$ between the scalar and the gauge-field mass. For superconductors, these mass scales correspond to the inverse correlation length and the inverse London penetration depth, respectively. For small values of the Higgs field mass, the phase transition is strongly enough first order to cutoff long-range fluctuations. This corresponds to the good type-I region for standard superconductors, $m_H/m_A<1$. On the other hand, the type-II region corresponds to $m_H/m_A>1$. Here, it is expected that the phase transition changes from first to second order.

A proper treatment of the long-range fluctuations is decisive for an understanding of the $U(1)$-Higgs phase transition as they change the effective interactions between the fields. The ''microscopic'' physics in the ultraviolet is characterized by the couplings at the short-distance length scale $1/\Lambda$ (or $\sim 1/T$, with $T$ the temperature). In turn, the physics close to a first-order phase transition depends typically on the (small) photon mass $m_A$, and thus requires the knowledge of the couplings at scales $\ll T$.[1]

A field-theoretical approach, which in principle is able to deal with the effects of long-range fluctuations and describes the related scaling of the couplings, is given by the Wilsonian renormalization group [3–6]. This procedure is based on integrating-out infinitesimal momentum shells about some ''coarse-graining'' scale $k$ within a (Euclidean) path-integral formulation. The infrared effective theory obtains, upon integrating, the resulting flow with respect to $k\to 0$. This way, the characteristic scaling behavior (or ''running'') of the couplings as functions of $k$, and in particular the running of the Abelian charge $e(k)$, is taken into account. A Wilsonian approach thus improves on perturbative resummations in that the perturbative expansion parameter $e^2T/m_A$ now becomes scale dependent, $e^2(k)T/m_A(k)$. While the former diverges close to a second-order phase transition, where the photon mass vanishes, the latter remains finite in the infrared, even for $m_A(k)\to 0$, due to the nontrivial scaling of the Abelian charge. The crucial role of running couplings in finite temperature phase transitions has been discussed in pure scalar theories [7,8].

In the present paper we employ the Wilsonian renormalization group to the type-I regime of the $U(1)$-Higgs phase transition. Our main contributions are twofold. First, we take into account the nontrivial scaling of the Abelian charge $e^2(k)$, characterized by an effective Abelian fixed point, which is kept as a free parameter. The infrared effects lead

*Email address: filf@stp.dias.ie
†Present address: Theory Division, CERN, CH–1211 Geneva 23, Switzerland. Email address: daniel.litim@cern.ch

[1]When speaking of ''scales'' we always have ''mass scales'' or ''momentum scales'' $\sim k$ in mind. The corresponding ''length scales'' are given as $\sim k^{-1}$.

 

the Abelian gauge coupling to crossover,[2] from its slow logarithmic running in the ultraviolet (effectively 4D) to a strong linear running in the infrared (effectively 3D). The characteristic scale for this crossover depends on the precise infrared (IR) behavior of the Abelian charge, and is decisive for both the strength of the transition and the properties of the phase diagram. This is currently the least well understood part of the problem. Equally important is to retain the full field dependence of the effective potential (no polynomial approximation), for which an analytical expression is given in the sharp cutoff case. We obtain all thermodynamical quantities related to the first-order phase transition and study their dependence on the crossover behavior. Second, we present a detailed quantitative analysis of the ''coarse-graining'' dependence of our results. This is an important consistency check for the method and the approximations involved. We give quantitative evidence for an intimate link between a truncation of the effective action, and the dependence on the coarse-graining scheme, which can simply be displayed as additional ''error bars'' due to the scheme dependence.

The 3D $U(1)$-Higgs phase transition has been studied previously using flow equations [9–13], and within perturbation theory [14–16]. Recent results from lattice simulations for both type-I and type-II regions have been reported as well [17,18]. In Ref. [9], the renormalization-group (RG) flow has been studied for the type-II regime within a local polynomial approximation for the effective potential about the asymmetric vacuum up to order $\phi^8$, in order to establish the phase diagram, the relevant fixed points, and the related critical indices. The polynomial approximation is expected to give reliable results for the scaling solution close to a second-order fixed point. The type-I regime has been discussed for the full potential, using a matching argument for the running of the Abelian charge. In Ref. [10], the large-$N$ limit and its extrapolation down to $N=1$, has been considered as well. It was pointed out that the local polynomial approximation becomes questionable close to a first-order phase transition or a tricritical fixed point at about $N\approx 4$ or smaller. This was later confirmed by Tetradis [12], who in addition abandoned the local polynomial approximation. The present paper, aimed particularly at the type-I region of the phase diagram, improves on Refs. [9,10] in that the full field dependence of the effective potential will be taken into account. A quantitative description of thermodynamical observables at the phase transition requires a good accuracy for the effective potential in the first place. Our paper also goes beyond the work of Ref. [12] in three important aspects. We study the dependence of physical observables on the value of the effective Abelian fixed point. In addition, explicit analytical solutions to approximate flow equations are given, as well as a discussion of the scheme dependence.

This paper is organized as follows. We introduce the Wilsonian flow equations and the particular Ansatz used for the $U(1)$-Higgs theory. The flows for the Abelian charge and the free energy are explained, as well as further approximations involved (Sec. II). We then proceed with the thermal initial conditions as obtained from perturbative dimensional reduction (Sec. III) and a discussion of the phase diagram and the critical line (Sec. IV). This is followed by a computation of all relevant thermodynamical quantities at the first-order phase transition as functions of the effective Abelian fixed point, a computation of the corresponding characteristic scales, and a discussion of the approximations made (Sec. V). A quantitative study of the scheme dependence on the main characteristics of the phase transition is given (Sec. VI), followed by a summary and an outlook (Sec. VII). Three Appendices contain some more technical aspects of our analysis.

## II. FLOW EQUATIONS

### A. Wilsonian flows

Wilsonian flow equations are based on the idea of a successive integrating out of momentum modes of quantum fields within a path-integral formulation of quantum-field theory [3,4]. This procedure, in turn, can also be interpreted as the step-by-step averaging of the corresponding fields over larger and larger volumes, hence the notion of coarse graining. The modern way of implementing a coarse-graining within a path-integral formalism goes by adding a suitable regulator term $\sim\int\phi R_k(q)\phi$, quadratic in the fields, to the action [5]. This additional term introduces a new scale parameter $k$, the coarse-graining scale. A Wilsonian flow equation describes how the coarse-grained effective action $\Gamma_k$ changes with the scale parameter $k$, relating this scale dependence to the second functional derivative of $\Gamma_k$ and the scale dependence of the IR regulator function $R_k$. The boundary conditions for the flow equation are such that the flow relates the microscopic action $S=\lim_{k\to\infty}\Gamma_k$ with the corresponding macroscopic effective action $\Gamma=\lim_{k\to 0}\Gamma_k$, the generating functional of one-particle irreducible Green's functions.

To be more explicit, we follow the ''effective average action'' approach as advocated in Ref. [5] and consider the flow equation

$$\frac{\partial}{\partial t}\Gamma_k[\Phi]=\frac{1}{2}\mathrm{Tr}\left\{(\Gamma_k^{(2)}[\Phi]+R_k)^{-1}\frac{\partial R_k}{\partial t}\right\}. \qquad (2.1)$$

Here, $\Phi$ denotes bosonic fields and $t=\ln k$ the logarithmic scale parameter. The length scale $k^{-1}$ can be interpreted as a coarse-graining scale [6]. The right-hand side of Eq. (2.1) contains the regulator function $R_k$ and the second functional derivative of the effective action with respect to the fields. The trace denotes a summation over all indices and integration over all momenta. The above flow interpolates between the classical and quantum effective action due to some properties of the regulator functions $R_k$ (see Sec. VI B). It is important to realize that the integrand of the flow equation (2.1), as a function of momenta $q$, is peaked about $q^2\approx k^2$, and suppressed elsewhere. Consequently, at each infinitesi-

[2]This crossover is not to be confused with the qualitatively different ''crossover'' observed in the type-II regime of $3+1$-dimensional $SU(2)+$Higgs theory.

mal integration step $k \to k - \Delta k$, only a narrow window of momentum modes contribute to the change of $\Gamma_k \to \Gamma_{k-\Delta k}$. In particular, modes with momenta $q \gg k$ no longer contribute to the running at the scale $k$. It is this property that justifies the interpretation of $\Gamma_k$ as a coarse-grained effective action with modes $q \gg k$ already integrated out.

For gauge theories, the flow equation (2.1) has to be accompanied by a modified Ward identity, which has to be satisfied at each scale $k$. Such a requirement is necessary to guarantee that the physical Green's functions obtained for $k \to 0$ obey the usual Ward identity [19–22]. Here, we use the background field formalism, as employed in Ref. [6] in the context of the effective average action with a covariant gauge fixing (Landau gauge).

The flow equation couples the infinite number of operators describing an effective action with its second functional derivative. In order to solve Eq. (2.1), one has to truncate $\Gamma_k$ to some finite number of operators relevant for the problem under investigation. Some systematic expansions for the flow equations are known. Apart from a weak-coupling expansion, which is known to reproduce the standard perturbative loop expansion, one can use expansions in powers of the fields, derivative expansions, or combinations thereof. These latter expansions have the advantage of not being necessarily restricted to a small coupling regime. A discussion on the use of a derivative expansion in Wilsonian RG is presented in Ref. [23].

We now turn to our Ansatz for the Abelian-Higgs model. The most important information regarding the phase structure of the model is encoded in the effective potential (or coarse-grained free energy) $U_k$, from which all further thermodynamical quantities are derived. Equally important is the wave-function renormalization factor of the gauge fields $Z_F$, which encodes the nontrivial running of the Abelian charge. In turn, the wave-function renormalization factor $Z_\varphi$ for the scalar fields, is less important because the scalar field anomalous dimension remains small in the type-I region of phase transitions. Hence, we approximate the effective action $\Gamma_k$ to leading order(s) in a derivative expansion through the following operators:

$$\Gamma_k[\phi,A] = \int d^dx \Big\{ U_k(\overline{\rho}) + \frac{1}{4} Z_{F,k} F_{\mu\nu} F_{\mu\nu} + Z_{\varphi,k} (D_\mu[A]\varphi)^* D_\mu[A]\varphi \Big\}, \tag{2.2}$$

where $\overline{\rho} = \varphi^* \varphi$, and $F_{\mu\nu} = \partial_\mu A_\nu - \partial_\nu A_\mu$ is the field strength of the electromagnetic field, and $D_\mu$ denotes the covariant derivative $\partial_\mu - ieA_\mu$.

In principle, the flow equation can be used directly (starting with initial parameters of the 4D theory at $T=0$) to compute the corresponding critical potential at finite temperature within the imaginary time formalism, or, like in Ref. [24], using a real-time formulation of the Wilsonian RG [25]. Our strategy, in the present case, is slightly simpler. We are interested in the region of parameter space, where the 4D couplings are small enough to allow a perturbative integrating out of the super-heavy and heavy modes, i.e., the nonzero Matsubara modes for all the fields and the Debye mode. In this case, we can rely on the dimensional reduction scenario and employ the results of Ref. [26], where the initial conditions were computed perturbatively. The result is then a purely three-dimensional theory for the remaining light degrees of freedom, whose infrared behavior is studied, applying the above Wilsonian renormalization group. In the sequel, we will therefore need the flow equations for $U_k$ and $e^2(k)$ in 3D. At the scale of dimensional reduction, that is the starting ultraviolet (UV) scale $\Lambda$ of the 3D-flow, we normalize the wave-function factors to one, and the initial effective potential $U_\Lambda$ is obtained from dimensional reduction.

### B. Cross-over of the gauge coupling

We now consider the case $d=3$, and discuss the flow for the Abelian coupling. A main feature of the Abelian Higgs theory in 3D is that the Abelian charge scales in a nontrivial manner with the coarse-graining scale $k$. The dimensionless Abelian charge in 3D is defined as

$$e_3^2(k) = \frac{\overline{e}_3^2(\Lambda)}{Z_F(k)k} \equiv \frac{\overline{e}_3^2(k)}{k}, \tag{2.3}$$

and its scale dependence is related to the gauge-field anomalous dimension $\eta_F = -\partial_t \ln Z_F(k)$ (here a function of $k$ and the fields) through [6]

$$\frac{de_3^2}{dt} = -e_3^2(1-\eta_F). \tag{2.4}$$

The first term in Eq. (2.4) comes from the intrinsic dimension of the charge squared (proportional to $k$), while the second term proportional to the gauge-field anomalous dimension, accounts for the nontrivial running of the coupling. The flow (2.4) always has the (trivial) Gaussian fixed point given by $e_3^2 = 0$. In addition, one might encounter further nontrivial fixed points that are given implicitly through the solutions of $\eta_F = 1$.

Both the scalar and the gauge-field anomalous dimensions, $\eta_\varphi$ and $\eta_F$, are perturbatively small near the Gaussian fixed point, i.e., $|\eta_\varphi|$ and $|\eta_F| \ll 1$. This holds true at the initial scale for $k=\Lambda$ in the effective 3D running, to be specified later. It follows that the running of the dimensionful Abelian charge is negligible near the Gaussian fixed point, $\overline{e}^2(k) \approx \overline{e}^2(\Lambda)$. Here, the dimensionless coupling scales as $e_3^2(k) \sim \Lambda/k$. In this regime it is expected that standard perturbation theory gives a reliable estimate of the effective potential in this region of the parameter space [13].

However, for $\eta_F < 1$, the Gaussian fixed point is IR unstable, as follows directly from Eq. (2.4). Therefore, when approaching the infrared, the dimensionless Abelian charge will unavoidably grow large, scaling away from the Gaussian fixed point. In particular, it can enter into a region, where $\eta_F(e^2)$ is no longer $\ll 1$. When a nontrivial fixed point is approached, i.e., $\eta_F \approx 1$, the suppression factor $(1-\eta_F)$ in Eq. (2.4) becomes important. A strong linear running of $\overline{e}^2 \sim k$ (the IR region is effectively $3d$) will ultimately set in as soon as the deviation from the Gaussian fixed point becomes

sizable [9,10,27]. In this regime, we expect some quantitative modifications of the predictions by perturbation theory due to the nontrivial running of the Abelian charge.

### C. Abelian fixed point

The anomalous dimension $\eta_F$ has been calculated in Ref. [6]. It is, in general, a complicated function of the gauge coupling, the fields, and the further parameter describing the effective action in a given approximation, like the coarse-grained potential (cf. Eq. (113) of Ref. [9]). However, $\eta_F$ is proportional to $e_3^2$ itself, and we write it as

$$\eta_F(\overline{\rho}) = \frac{e_3^2}{e_\star^2(\overline{\rho})}. \tag{2.5}$$

Given the anomalous dimension, Eq. (2.5) provides a definition of $e_\star^2(\overline{\rho})$. Our current understanding of the IR behavior of the gauge sector, hinges on the precise properties of $\eta_F(\overline{\rho})$, and hence of $e_\star^2(\overline{\rho})$.

Let us recall a few cases where $e_\star^2$ is approximately known. First, within standard perturbation theory, the dimensional gauge coupling $\overline{e}_3^2 = e_3^2 k = \text{const}$ throughout. Within our formalism, the ''no running'' corresponds to the limit $e_\star^2 \to \infty$. In this limit, the effective fixed point is independent of the fields and we can expect to be close to the results from perturbation theory, as long as additional effects due to the scalar anomalous dimension, can be neglected.[3]

Second, consider the large-$N$ limit of the $U(1)$-Higgs model, where $N$ denotes the number of complex scalar fields. In this limit, the flow (2.4) is dominated by the contributions of the Goldstone modes. They overwhelm those due to the radial mode. Therefore, $e_\star^2$ becomes

$$e_\star^2 \approx \frac{6\pi^2}{N} \tag{2.6}$$

close to the minimum of the effective potential.[4] In particular, Eq. (2.6) no longer depends on the quartic scalar coupling or the location of the vacuum expectation value (VEV) because the massive (radial) mode is suppressed. Extrapolating (2.6) down to the physically relevant case $N=1$, corresponds to replacing the radial mode by a massless one. This yields $e_\star^2 \approx 6\pi^2$, in accordance with the leading-order result from the $\epsilon$ expansion. This value serves as a reference value for our subsequent considerations.

Third, we recall the findings of Refs. [9] and [10], where the function $\eta_F$ has been studied numerically for different $N$ within a local polynomial approximation of the flow about the nontrivial minimum at $\overline{\rho} = \overline{\rho}_0$ (up to $\sim \phi^8$). It was found that the implicit solutions to $\eta_F(e_\star^2) = 1$ for small $N$ (in particular $N=1$) can deviate considerably from the large-$N$ extrapolation $6\pi^2$. This deviation is due to the decoupling effects of the massive mode. Still, the qualitative form of Eq. (2.5), where the function $e_\star^2$ is replaced by an effective field-independent fixed point, remains a good approximation to Eq. (2.5). This simplified picture persists if the field derivatives $\partial \ln[e_\star^2(\overline{\rho})]/\partial\overline{\rho}$ remain small within the nonconvex region of the effective potential (see also the discussion in Sec. V E). This implies that the threshold effects of the radial mode for $N=1$ act on Eq. (2.4) by varying the number of scalar fields in Eq. (2.6).

Hence, the qualitative structure of the flow (2.4), to leading order, is determined by Eq. (2.5) with $e_\star^2$ given by some number, e.g., the appropriate effective fixed point. For the present purpose, it is sufficient to study the flow (2.4) with $e_\star^2$ as a free parameter. The properties of the first-order phase transition depend on the size of $e_\star^2$. However, as we shall see in detail below, the dependence turns out to be very small for large $e_\star^2$; this part of the phase diagram can be studied without having a complete understanding of the underlying fixed-point structure. In turn, we find a strong dependence within regions where the effective fixed point is small. For this case, a more refined analysis is required in order to provide more reliable predictions.

### D. Crossover scale

Within the remaining part of the paper we approximate the anomalous dimension as described above. Hence, the Eqs. (2.4) and (2.5) are easily solved by

$$e_3^2(k) = \frac{e_\star^2}{1 + k/k_{\rm cr}}. \tag{2.7}$$

We note the appearance of a characteristic *crossover scale*

$$k_{\rm cr} = \frac{\Lambda e_3^2(\Lambda)}{e_\star^2 - e_3^2(\Lambda)}. \tag{2.8}$$

It describes the crossover between the Gaussian and the Abelian fixed point, and depends on the initial conditions. For $k > k_{\rm cr}$, the running is very slow and dominated by the Gaussian fixed point, $\overline{e}_3^2(k) \sim \text{const}$. This corresponds also to the limit $e_\star^2 \to \infty$. On the other hand, for $k < k_{\rm cr}$, the running becomes strongly linear and the Abelian fixed point governs the scale dependence $\overline{e}_3^2(k) \sim k$. The question as to how strong the first-order phase transition is affected by this crossover, depends on whether the crossover scale is much larger (strong effect) or much smaller (weak effect) than the typical scales of the transition (see Sec. V D). The crossover scale turns negative if the initial value $e_3^2(\Lambda)$ is too big. This simply means that the flow would never be dominated by the Gaussian fixed point (see Fig. 1) in the first place (no crossover). Although this case is interesting in its own right, this region will not be discussed any further.

[3] In the region where $\lambda \gg e^2$ (e.g., strongly type-II superconductors), the critical behavior of the limit $e_\star^2 \to \infty$ corresponds to an effective scalar theory, which belongs to a different universality class than the $O(2N)$ scalar theory obtained for $e_\star^2 \to 0$ [9].

[4] In Eq. (2.6), ''$\approx$'' means equality up to a regulator scheme dependent coefficient of $\mathcal{O}(1)$.

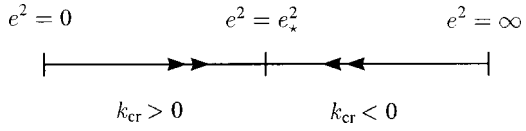


FIG. 1. The relation between the sign of the crossover scale $k_{\rm cr}$ and the running of the gauge coupling (arrows indicate the direction of the $e^2$ flow as $k\to 0$).

### E. The running potential

We now turn to the flow equation for the effective potential, which can be obtained from the flow equation (2.1) using the Ansatz given by Eq. (2.2). The resulting flow equation is a second-order nonlinear partial differential equation. It has been derived originally in Ref. [6] and reads in 3D

$$\frac{4\pi^2}{k^2}\frac{d}{dk}U_k(\bar\rho)=(2N-1)l_0^3\left(\frac{U_k'(\bar\rho)}{k^2}\right)+l_0^3\left(\frac{U_k'(\bar\rho)+2\bar\rho U_k''(\bar\rho)}{k^2}\right)+2l_0^3\left(\frac{2\bar e_3^2(k)\bar\rho}{k^2}\right) \tag{2.9}$$

for the case of $N$ complex scalar fields. Similar flow equations are obtained for the wave-function factors $Z_\varphi$ and $Z_F$, and thus for the anomalous dimensions $\eta_\varphi=-\partial_t\ln Z_\varphi$ and $\eta_F=-\partial_t\ln Z_F$. Here, $l_0^3(\omega)$ denotes a scheme dependent threshold function defined as

$$l_n^d(\omega)=-(\delta_{n,0}+n)\int_0^\infty dy\,\frac{r'(y)y^{1+d/2}}{[y(1+r)+\omega]^{n+1}}. \tag{2.10}$$

These functions have a pole at some $\omega<0$ and vanish for large arguments. The function $r(q^2/k^2)$ is related to the regulator function $R_k$ introduced in Eq. (2.1) through

$$R_k(q^2)=Zq^2r(q^2/k^2), \tag{2.11}$$

where $Z$ denotes either the scalar or gauge-field wave-function renormalization.[5]

We can distinguish three different contributions to the running of the potential (2.9), which are, from the left to the right, related to the massless scalar, massive scalar, and the gauge-field fluctuations, respectively. Not all the three of them are of the same order of magnitude, though. Indeed, it was already noted [28] that the gauge-field fluctuations dominate (2.9) if the quartic scalar coupling $\lambda$ is much smaller than the gauge coupling squared, $\lambda/e^2\ll 1$. This is the case for the physically relevant initial conditions, that is, for the starting point of the flow equation (2.9). Therefore, we can make a further approximation and neglect the contributions from the scalar field fluctuations compared to those from the gauge field. The flow equation thus takes the form

$$\frac{2\pi^2}{k^2}\frac{d}{dk}U_k(\bar\rho)=l_0^3\left(\frac{2\bar e_3^2(k)\bar\rho}{k^2}\right). \tag{2.12}$$

Integrating the approximated flow equation allows to control self-consistently whether the effects from scalar fluctuations remain negligible or not. It suffices to evaluate the right-hand side of Eq. (2.9) with $U_k$ from the solution of Eq. (2.12) to compare the contribution of the neglected terms to the running of, say, $U_k''$ with the leading contributions. It is well known that the scalar fluctuations are important for the inner part of the effective potential, which becomes convex in the limit $k\to 0$ [29]. Therefore, it is to be expected that this approximation becomes unreliable, within the nonconvex part of the potential, at some scale $k_{\rm flat}$.

The solution to Eq. (2.12) is the first step of a systematic iteration to compute the solution to Eq. (2.9). The next step would be to replace $U_k$ on the right-hand side of (2.9) by the solution to Eq. (2.12). Proceeding to the next iteration step, the scalar fluctuations are eventually taken into account. Solving Eq. (2.9) with $U_k$ on the right-hand side replaced by the explicit solution of Eq. (2.12), is much easier than solving Eq. (2.9) directly, because the former becomes an ordinary differential equation, while the latter is a partial one. This procedure can be interpreted as an expansion in terms of scalar loops around the gauge-field sector. We will mainly use the first step in the sequel. In order to estimate the integrated contribution of the scalar fluctuations, we will in addition discuss the solution of (2.9) with $U_k$ on the right-hand side replaced by $U_\Lambda$ (see Appendix C).

### F. The coarse-grained free energy

The coarse-grained free energy is obtained as the solution to the coupled set of flow equations (2.4) and (2.9). In the present case, a solution can be written as

$$U_k(\bar\rho)=U_\Lambda(\bar\rho)+\Delta_k(\bar\rho). \tag{2.13a}$$

Here, the term $\Delta(\bar\rho)$ stems from integrating out the 3D fluctuations between the scales $\Lambda$ and $k$. With $e_3^2(k)$ from Eq. (2.7) and $dU_k/dk$ from Eq. (2.12), it reads

$$\Delta_k(\bar\rho)=\frac{1}{2\pi^2}\int_k^\Lambda d\bar k\int_0^\infty dy\,\frac{r'(y)y^{5/2}\bar k^3(1+\bar k/k_{\rm cr})}{y\bar k(1+r)(1+\bar k/k_{\rm cr})+2e_\star^2\bar\rho}+\text{const.} \tag{2.13b}$$

The constant is fixed by requiring that $\Delta_k(0)=0$. In Eq. (2.13b) we see that the term resulting from integrating out 3D effective modes, depends on the RS through the regulator function $r(y)$ and its first derivative. (Explicit expressions are given in Appendix B.) The above expressions are enough to study all properties of the phase transitions as functions of the parameters of the potential $U_\Lambda$.

We are aiming to use an initial condition at $k=\Lambda$ obtained from perturbation theory in 4D. This requires that the parametrization of the 3D potential $U_\Lambda$ is such that the matching equates the right parameters. In the universal limit

[5]A more detailed discussion of both $R_k$ and the dimensionless functions $r(q^2/k^2)$ is postponed until Sec. VI B.

$\Lambda\to\infty$, the effective-mass term contained via $U_\Lambda$, is renormalized to $U_\Lambda\to U_\Lambda - C_\Lambda\bar{\rho}$. For a sharp cutoff, we find explicitly

$$C_\Lambda(e)=\frac{e_\star^2}{\pi^2}[\Lambda k_{\rm cr}-k_{\rm cr}^2\ln(\Lambda/\Lambda_0)]. \tag{2.14}$$

For finite $\Lambda$, this corresponds to a finite renormalization of the parameters of the theory, i.e., the mass term, or, equivalently, a finite shift of the VEV at the matching scale.[6] This finite renormalization has its origin simply in the way the flow equation integrates out the 3D momentum scales. Only after this transformation will it be appropriate to identify the potential $U_\Lambda$ at the scale of dimensional reduction with the renormalized effective potential obtained from a perturbative calculation.

## III. THERMAL INITIAL CONDITIONS

We now specify, in concrete terms, the initial conditions for the effective 3D theory. The task is to relate the 3D renormalized parameters of the effective potential to those of the $T=0$ 4D theory. The initial conditions for the 3D running are the potential $U_\Lambda(\bar{\rho})$ and the gauge coupling $\bar{e}_3^2(\Lambda)$. The effective perturbative 3D Lagrangian has been derived in Ref. [26]. We start with the 4D effective action

$$\Gamma[\phi,A]=\int d^4x\left\{\frac{1}{4}F_{\mu\nu}F_{\mu\nu}+(\mathcal{D}_\mu\phi)^\dagger(\mathcal{D}_\mu\phi) - \frac{m_H^2}{2}\phi^\dagger\phi+\frac{\lambda}{2}(\phi^\dagger\phi)^2\right\}, \tag{3.1}$$

where $\phi$ is a single-component 4D complex scalar field. The mass parameter $m_H$ entering Eq. (3.1), denotes the $T=0$ Higgs boson mass. It is related to the other zero-temperature parameters of the theory by

$$\frac{\lambda}{e^2}=\frac{m_H^2}{M_W^2} \tag{3.2}$$

with $M_W$ the photon mass. In the phase with spontaneous symmetry breaking, $m_H^2>0$, we have $\langle\phi^*\phi\rangle\equiv v^2/2 = M_W^2/2e^2$. The effective action for the 3D theory obtains as

$$\Gamma_\Lambda[\varphi,A]=\int d^3x\left\{\frac{1}{4}F_{ij}F_{ij}+(\mathcal{D}_i\varphi)^\dagger(\mathcal{D}_i\varphi)+V_\Lambda(\bar{\rho})\right\}, \tag{3.3a}$$

$$V_\Lambda(\bar{\rho})=m_3^2\varphi^\dagger\varphi+\frac{\bar{\lambda}_3}{2}(\varphi^\dagger\varphi)^2, \tag{3.3b}$$

where $\varphi$ is the static component of $\phi$ and $i,j$ are the spatial components of $\mu,\nu$. The electric component of the gauge field has been fully integrated out because it acquires a thermal (Debye) mass $m_D$. The effects of the fluctuation of this mode are suppressed by inverse powers of $T$ as $m_D\propto T$, like the nonstatic modes. Following Ref. [26], the matching conditions read to one-loop accuracy

$$\bar{e}_3^2(\Lambda)=e^2T, \tag{3.4a}$$

$$\bar{\lambda}_3(\Lambda)=\left(\lambda+\frac{e^4}{4\pi^2}\right)T-\frac{e^4}{4\pi}\frac{T^2}{m_D(\Lambda)}, \tag{3.4b}$$

$$m_3^2(\Lambda)=\left(\frac{1}{4}e^2+\frac{1}{6}\lambda\right)T^2-\frac{1}{2}m_H^2-\frac{e^2}{4\pi}m_D(\Lambda), \tag{3.4c}$$

$$m_D^2(\Lambda)=\frac{1}{3}e^2T^2. \tag{3.4d}$$

Using the above, and taking into account the finite renormalization (2.14), as explained in Sec. II F, the renormalized effective initial potential $U_\Lambda(\bar{\rho})$ entering Eq. (2.13a) can be expressed in terms of the $T=0$ parameters and Eq. (3.4) as

$$U_\Lambda(\bar{\rho})=-m_R^2\bar{\rho}+\frac{1}{2}\bar{\lambda}_R\bar{\rho}^2 \tag{3.5a}$$

with

$$m_R^2(\Lambda)=\frac{1}{2}m_H^2-\left(\frac{e^2}{4}+\frac{\lambda}{6}-\frac{e^3}{4\sqrt{3}\pi}\right)T^2+C_\Lambda(e), \tag{3.5b}$$

$$\bar{\lambda}_R(\Lambda)=\left(\lambda+\frac{e^4}{4\pi^2}-\frac{\sqrt{3}e^3}{4\pi}\right)T, \tag{3.5c}$$

and the dimensionless renormalized quartic coupling reads $\lambda_R=\bar{\lambda}_R/\Lambda$. The renormalized VEV at the scale of dimensional reduction follows as

$$\bar{\rho}_R(\Lambda)=m_R^2(\Lambda)/\bar{\lambda}_R(\Lambda). \tag{3.5d}$$

All the 3D parameters are now defined at the reduction scale $\Lambda$, which is on dimensional grounds, linearly related to the temperature:

$$\Lambda=\xi T. \tag{3.6}$$

Using Eqs. (2.8), (3.4a), and (3.6) it follows, that the crossover scale $k_{\rm cr}$ is also related to $T$ as

$$k_{\rm cr}=\frac{\xi e^2}{\xi e_\star^2-e^2}T. \tag{3.7}$$

Let us finally comment on the matching parameter $\xi$. On one hand, $\xi$ has to be smaller than $2\pi$, because elsewise the assumption that all heavy modes have been integrated out, can no longer be maintained. On the other hand, a too small value for $\xi$, say $\xi<1$, would tend to neglect contributions from modes roughly within the window $\approx 2\pi T$ and $\approx T$. For the problem under consideration, $\xi\approx 1$ turns out to be a good

[6] This shift corresponds to the finite renormalization as employed in Ref. [12].

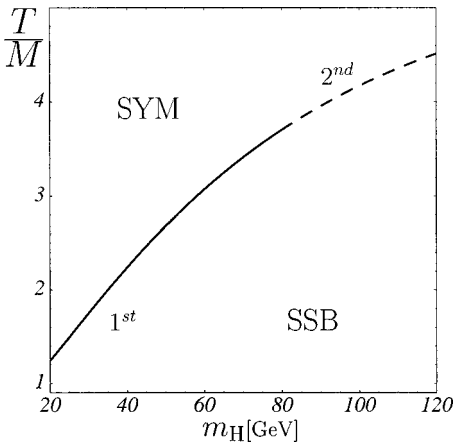


FIG. 2. The phase diagram in the $(T,m_H)$ plane.

choice. This choice shall be adopted throughout. Our results do depend very little on a variation of this matching scale (see also the comment in Sec. V D below).

## IV. THE PHASE DIAGRAM AT FINITE TEMPERATURE

We have now all the ingredients to study in detail the phase diagram and the phase transition of scalar electrodynamics. In this section, we discuss the main characteristics of the phase diagram as well as some properties of the critical line. The following section collects our results for the thermodynamical quantities related to the first-order phase transition and a discussion of the characteristic scales of the problem.

### A. The phase diagram

The ''phases'' of scalar electrodynamics are distinguished by the location of the global minimum of the effective potential. Above the critical temperature, the ground state corresponds to vanishing field $\bar{\rho}_0=0$, that is, to the symmetric phase. Below the critical temperature, the ground state corresponds to $\bar{\rho}_0\neq 0$, the phase with spontaneous symmetry breaking (SSB).[7] The corresponding phase diagram in the $(T,m_H)$-plane is displayed in Fig. 2. The phase transition between these two phases is first order for small $\bar{\lambda}_3/\bar{e}_3^2$, that is for small values of the Higgs field mass. In the context of superconductivity this region corresponds to the strongly type-I systems. For very large Higgs field mass, the phase transition turns second or higher order [9].[8]

In Fig. 3, we have displayed the coarse-grained free energy within the type-I region of parameters for $m_H=60\,\mathrm{GeV}$ for different scales and temperatures. At the critical temperature (left panel), it is realized that a barrier is building up for decreasing scale $k$, eventually creating a second minima at the vanishing field. The minima are degenerate in the infrared limit $k\approx k_{\mathrm{stable}}$ (that corresponds roughly to $k\to 0$ in the present approximation). Notice that the flattening of the inner part of the potential is not observed because the scalar fluctuations have been neglected at the present state. Rather, the effective potential reaches the degenerate shape already at some scale $k_{\mathrm{stable}}$, which should be larger than the scale where the flattening sets in.[9]

The temperature dependence of the coarse-grained free energy at $k\approx k_{\mathrm{stable}}$ is shown in the right panel of Fig. 3. The metastability range $\Delta T=T_s-T_b$ between the barrier temperature $T_b$, where the potential develops a second minimum at the origin (lowest-dashed curve) and the spinodal temperature $T_s$, where the asymmetric minimum disappears (uppermost dashed curve), is very small.

The physical quantities that characterize a first-order phase transition (except the metastability range) are defined at the critical temperature $T_c$, when the potential has two degenerate minima, the trivial one at $\bar{\rho}=0$, and a nontrivial one at $\bar{\rho}=\bar{\rho}_0\neq 0$. The critical line of the phase diagram as depicted in Fig. 2 is obtained solving the criticality conditions

$$0=\left.\frac{dU_k}{d\bar{\rho}}\right|_{\bar{\rho}=\bar{\rho}_0}, \tag{4.1a}$$

$$U_k(0)=U_k(\bar{\rho}_0). \tag{4.1b}$$

Here we kept $k$ arbitrary, though strictly only for $k=0$ are these conditions required physically. They establish a relationship between the parameters of the theory, and thereby define the critical line between the symmetric and the SSB phase in Fig. 2. It is helpful to rewrite the conditions (4.1) into

$$F_1(\bar{\rho}/T)=\lambda_R, \tag{4.2a}$$

$$F_2(\bar{\rho}/T)=2\frac{m_R^2}{T^2}. \tag{4.2b}$$

The functions $F_1$ and $F_2$ are related to the fluctuation integral through

$$F_1(x)=\frac{2}{x^2}[\tilde{\Delta}(x)-x\tilde{\Delta}'(x)], \tag{4.3a}$$

$$F_2(x)=\frac{2}{x}[2\tilde{\Delta}(x)-x\tilde{\Delta}'(x)], \tag{4.3b}$$

with

$$\tilde{\Delta}(\bar{\rho}/T)=\Delta(\bar{\rho})/T^3. \tag{4.3c}$$

[7]It is sensible to speak of two distinct phases only for $N>1$ complex scalar fields. For $N=1$, the symmetry is never broken in the strict sense. However, we will stick to the usual—albeit slightly incorrect—terminology even for $N=1$.

[8]The strongly type-II region has been studied using flow equations within a local polynomial approximation in Ref. [9]. See also Ref. [12].

[9]A quantitative discussion of these scales is given in Sec. V D below.

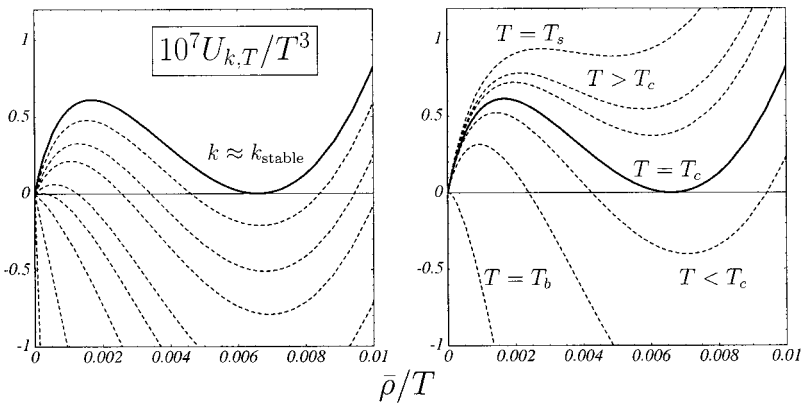


FIG. 3. The coarse-grained free energy as a function of the scale parameter and the temperature ($m_H = 60$ GeV). The full line corresponds to $T = T_c$ and $k \approx k_{\rm stable}$. Left panel: $T = T_c$, for different scales $k$. Right panel: $k \to k_{\rm stable}$, for different temperatures around $T_c$.

The first condition determines the ratio $x = \bar{\rho}/T_c$ of the discontinuity to critical temperature in dependence on the 4D parameters as given through $\lambda_R(e,\lambda)$ from Eq. (3.5c). The second one relates the solution of Eq. (4.2a) to the ratio of the Higgs boson mass to critical temperature and Eq. (3.5b), and eventually to the critical temperature and the discontinuity itself. Explicit expressions for the scale-dependent effective potential and the function $\Delta(\bar{\rho})$ are given in the Appendix B.

### B. Endpoint of the critical line

Some simple properties of the solutions to Eq. (4.2) can be deduced directly from the functions $F_{1,2}$. For $x > 0$, these functions [with $\Delta_k$ from Eq. (B5)] are positive, finite, monotonically decreasing, and vanishing for $x \to \infty$. They reach their respective maxima at $x = 0$, with (for $k = 0$)

$$F_1(0) = \frac{2}{\pi^2} e_\star^2 e^2, \tag{4.4a}$$

$$F_2(0) = \frac{2}{\pi^2} \frac{\xi^2 e_\star^2 e^2}{\xi e_\star^2 - e^2} \left[ 1 - \frac{e^2}{\xi e_\star^2 - e^2} \ln\left( \xi \frac{e_\star^2}{e^2} \right) \right]. \tag{4.4b}$$

The renormalized 3D quartic coupling $\lambda_R$, as given by Eq. (3.5c) and fixed through the 4D parameters of the theory, is positive in the domain under consideration. Given the monotony property of $F_1$, it follows that a solution to Eq. (4.2a) is unique (if it exists). There exists no solution for too large values of $\lambda_R$. Its largest possible value corresponds to vanishing VEV, i.e., to $x = 0$. Using Eqs. (3.2) and (3.5c) gives an upper bound on the scalar mass when the phase transition is first order. It reads

$$\frac{m_H^2}{M_W^2} \leqslant \frac{2 e_\star^2}{\pi^2}. \tag{4.5}$$

For any finite value of $e_\star^2$, Eq. (4.5) predicts an upper limit for the mass of the Higgs particle. This is an immediate consequence of the existence of an effective fixed point for the running gauge coupling (2.4). Indeed, as the limit $e_\star^2 \to \infty$ corresponds to perturbation theory, we recover the standard perturbative prediction of a first-order phase transition for all Higgs boson mass. This endpoint is usually interpreted as the tricritical point of the model, above which the phase transition turns from a first-order transition to a second-order one. However, the endpoint of the first-order transition line is within the domain of validity of the present computation only for sufficiently small values of $e_\star^2$.[10] For larger values of the Abelian fixed point, we expect that the precise location of the endpoint is also determined by the scalar field fluctuations.

In the opposite case, the smallest possible value for $\lambda_R$ corresponds to $x \to \infty$, thus to $\lambda_R = 0$. This gives a lower bound on the mass of the Higgs particle according to

$$\frac{\sqrt{3} e}{4\pi} < \frac{m_H^2}{M_W^2}. \tag{4.6}$$

For $M_W = 80.6$ GeV and $e = 0.3$, the bound is satisfied at about $m_H \approx 16$ GeV. This bound stems entirely from the initial conditions employed. This indicates that the dimensional reduction scenario is no longer appropriate for small $m_H$. In the present paper, we are also not interested in the region of parameter space where the Coleman-Weinberg mechanism already takes place within the original 4D theory, which happens at even smaller values for $m_H$ (typically for $\lambda/e^4$ at about $3/8\pi^2$ or smaller [27]).

## V. THERMODYNAMICS OF THE FIRST-ORDER PHASE TRANSITION

Here we present our results for the coarse-grained free energy and related physical quantities close to the critical temperature of the first-order phase transition as a function of the effective Abelian fixed point. The initial conditions are specified through the gauge coupling at vanishing temperature $e = 0.3$ and the photon mass $M_W = 80.6$ GeV. The ratio $\lambda/e^2$ of the 4D couplings ranges between 0.06–0.75 for a Higgs field mass between 20–70 GeV. Relevant information is given by the critical temperature $T_c$, the discontinuity at the phase transition $\bar{\rho}_0$, the latent heat $L$, and the surface tension $\sigma$.[11] We compare our findings to perturbation theory,

[10] The end point presented in Fig. 2 corresponds to $e_\star^2 \approx 5$.

[11] A comment concerning the dimensions is in order: $U$, $\sigma$, $L$, and $\bar{\rho}$ will be given in 3D units, unless otherwise started. Their 4D counterparts are simply obtained by multiplying with $T$.

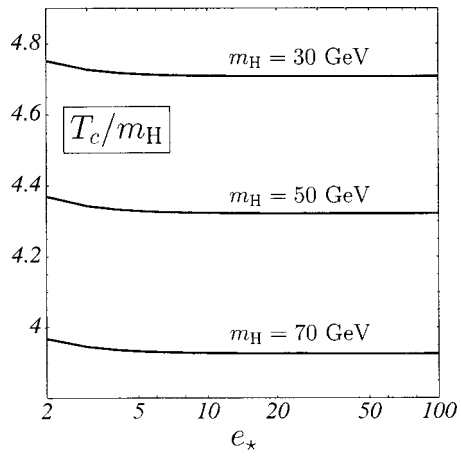


FIG. 4. The critical temperature as a function of the Abelian fixed point.

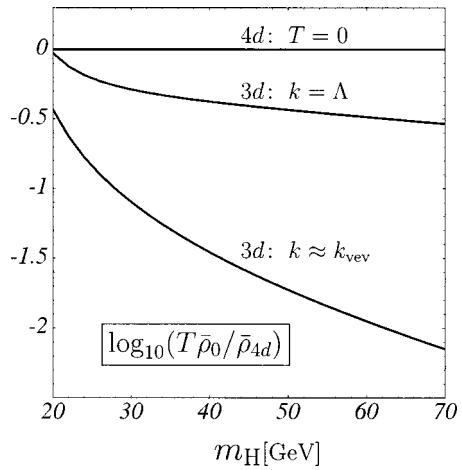


FIG. 5. The size of the VEV $\overline{\rho_0}(k)$ at $T=0$, $k=\xi T$, and at $k\approx k_{\rm VEV}$ (in units of the 4D VEV $\overline{\rho}_{4d}$ at $T=0$).

and to lattice simulations (for the critical temperature). All our results are obtained as functions of the effective fixed point of the Abelian charge. Due to the approximations performed, they depend also on the regularization scheme. We use a sharp cutoff regulator throughout the present section. The regularization scheme dependence is discussed in the following section.

### A. Discontinuity and critical temperature

We begin with the discontinuity and the critical temperature, which follow directly from solving the criticality conditions (4.2). The critical temperature as a function of the Abelian fixed point is given in Fig. 4 for $m_H=30$, 50, and 70 GeV. It turns out that $T_c$ is rather insensitive against $e_\star^2$. We observe an effect of a few percent only for very small values of $e_\star^2$ (see also Fig. 15). This is not a feature of the Higgs mass being relatively small, as similar results are obtained for all $m_H$.

Before continuing, let us briefly compare our findings for the critical temperature to existing lattice data. Lattice results have been reported for $e=\frac{1}{3}$, $m_W=80.6$ GeV, and $m_H=30$ GeV for the noncompact $U(1)$-Higgs model in Ref. [17], and for the compact one in Ref. [18]. The result reported in Ref. [17] is $T_c=131.18$ GeV for a finite lattice spacing. The continuum limit gives the slightly lower value $T_c=130.86$ GeV [18]. This is consistent with $T_c=131.28$ GeV, the result for the compact case [18]. Here, for $e_\star^2=6\pi^2$, we find $T_c=128.11$ GeV. As shown in Fig. 4, the critical temperature is essentially independent of the effective Abelian fixed point. The perturbative value is $T_c=132.64$ GeV [17]. These results are in good numerical agreement.

We now turn to the discussion of the discontinuity. In Fig. 5 we compare the logarithm of the VEV in 4D units (normalized to the VEV at $T=0$) at different scales. The renormalization of $\overline{\rho_0}$ between the $T=0$ and the $k=\Lambda$ lines, results from the integration of the heavy and super-heavy modes, given by Eq. (3.5d). The scale $k_{\rm VEV}$ is defined as the scale where the running of the potential minimum stops. This scale is related to the scale $k_M$, where the photon mass in the SSB regime is becoming larger than the coarse-graining scale, and thus decouples. Indeed, in the present approximation, the flow equation for the potential minimum reads

$$\frac{d\overline{\rho_0}}{dk}=\frac{1}{\pi^2}\frac{\overline{e}^2(k)}{\overline{\lambda}(k)}l_1^3[M^2(k)/k^2]. \tag{5.1}$$

Here, $\overline{\lambda}(k)=U_k''[\overline{\rho_0}(k)]$ denotes the quartic coupling at the minimum, and

$$M^2(k)=2\overline{e}^2(k)\overline{\rho_0}(k) \tag{5.2}$$

the photon mass squared. The running of the VEV decouples at $k\approx k_{\rm VEV}$, which happens as soon as the 3D photon mass $M$ is sufficiently larger than the scale $k$ (roughly at $M^2/k^2\approx 10$) such that the threshold function in Eq. (5.1) suppresses any further renormalization ($k_{\rm VEV}/T$ is displayed in Fig. 12).

From Fig. 5, we conclude that the main part of the actual running of the potential minimum comes from integrating out the 3D fluctuations, as can be inferred from the wide separation of the $k=\Lambda$ and the $k\approx k_{\rm VEV}$ lines as opposed to the comparatively narrow separation of the $T=0$ and the $k=\Lambda$ lines.

Figure 6 shows the VEV $\overline{\rho_0}$ as a function of the Higgs field mass and the Abelian fixed point. The shaded region covers the region $2\leqslant e_\star\leqslant\infty$ for the Abelian fixed point value. For small $m_H$, the effect is clearly negligible. With increasing $m_H$, however, the influence of the running gauge coupling is increasing drastically, leading to a strong weakening of the phase transition (see also Fig. 15).

Finally we compare in Fig. 7, the ratio of the 4D VEV $\phi_0$ to the initial $T=0$ VEV $v/\sqrt{2}$ for different Abelian fixed point values with the findings of perturbation theory.[12] Again, the shaded region covers the region $2\leqslant e_\star\leqslant\infty$ for the Abelian fixed point. We observe that the VEV shows a small dependence on the Abelian fixed point for sufficiently small Higgs field mass. For larger values of $m_H$, the VEV ap-

[12]We thank A. Hebecker for providing his data from Ref. [15] for comparison in Figs. 7, 9, 10, and 11.

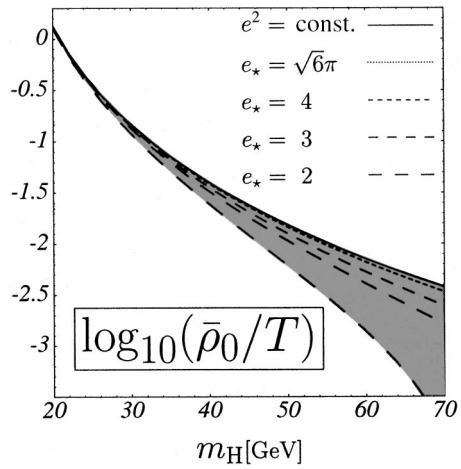


FIG. 6. The 3D VEV $\overline{\rho_0}$ as a function of the Abelian fixed point.

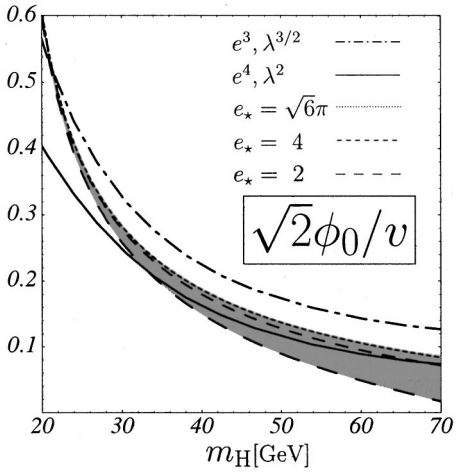


FIG. 7. The VEV for various values of the Abelian fixed point in comparison with perturbation theory to order $(e^3,\lambda^{3/2})$ and $(e^4,\lambda^2)$.

proaches the perturbative two-loop result. It follows that the VEV is rather stable against effects from the running Abelian charge, say at least for $e_\star^2 > 20$. Only for $e_\star^2 \approx 4$, the running becomes strong enough to result in a significant decrease of $\overline{\rho_0}$.

### B. The critical potential

The critical potential is shown in Figs. 8 and 9 for $m_H = 38$ GeV. Figure 8 gives the critical potential in units of the critical temperature for different values of $e_\star^2$ as functions of $\overline{\rho}/T$.[13] We note that for large $e_\star^2 > 6\pi^2$, the shape of the potential is rather insensitive against a change in $e_\star^2$. Here, the additional scale dependence induced through the gauge coupling is quite small (a few percent). For small values of $e_\star^2$, the height of the barrier is reduced significantly, up to a factor of 3 at $e_\star^2 = 4$. The strong scaling of $\overline{e^2}$ thus weakens the phase transition considerably for small $e_\star^2 \ll 6\pi^2$. Again, the quantitative change depends strongly on the value for the effective Abelian fixed point, if $e_\star^2 \ll 6\pi^2$. The nontrivial running of $\overline{e^2}(k)$ has a stronger effect on the small $\overline{\rho}$ region of the potential. Here, the decoupling of the gauge field sets in only at smaller scales, which in turn results in a stronger quantitative effect due to the running gauge coupling.

Figure 9 gives the critical potential in units of the 4D VEV $v/\sqrt{2}$, and compares the solution of Eq. (2.12) with those obtained within perturbation theory (PT). Line (a) corresponds to PT at order $(e^3,\lambda^{3/2})$ [14], line (b) to our result with $e_\star^2 = 6\pi^2$, line (c) to PT at order $(e^4,\lambda^2)$ [15], and line (d) to our result with $e_\star^2 = 4$. For $e_\star^2 = 6\pi^2$, the critical potential is situated halfway between the one- and two-loop perturbative results. For decreasing $e_\star^2$, the critical potential approaches quickly the two-loop result, and becomes even smaller at about $e_\star^2 \approx 4$. It is interesting to note that a value for $e_\star^2$ can be found for which the two-loop perturbative result is matched perfectly.

### C. Surface tension and latent heat

The interface tension for a planar interface separating the two degenerate vacua follows from Eq. (2.2) as

$$\sigma = 2\int_0^{\varphi_0} d\varphi \sqrt{Z_\varphi U_{\rm crit}(\overline{\rho})}. \tag{5.3}$$

It is sensitive to the actual shape of the critical potential and yields additional information regarding the strength of the phase transition. In Fig. 10 the surface tension is shown as a function of $m_H$ and in comparison with perturbation theory. The shaded region covers the results for $2 \leqslant e_* \leqslant \sqrt{6}\pi$. We again note that the effect of the running coupling is negligible for small Higgs boson mass. In contrast to the VEV, the surface tension depends rather strongly on $e_\star^2$, already for moderate values of $m_H$. An even stronger running of $e_3^2$

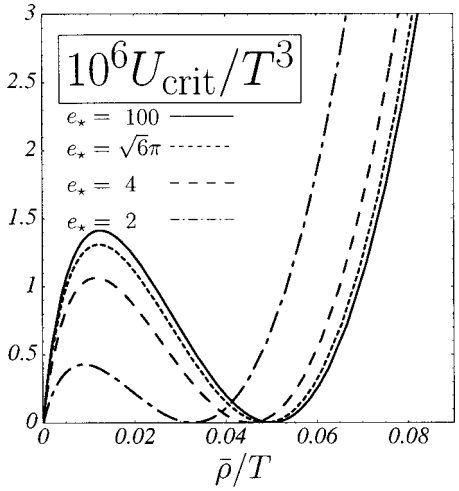


FIG. 8. The critical potential for different values of the effective fixed point.

[13]Notice that comparing critical potentials (or other relevant quantities) in units of $T$ for different values of $e_\star^2$, is sensible due to the very weak dependence of $T_c$ on the effective fixed point (see Figs. 4 and 15).

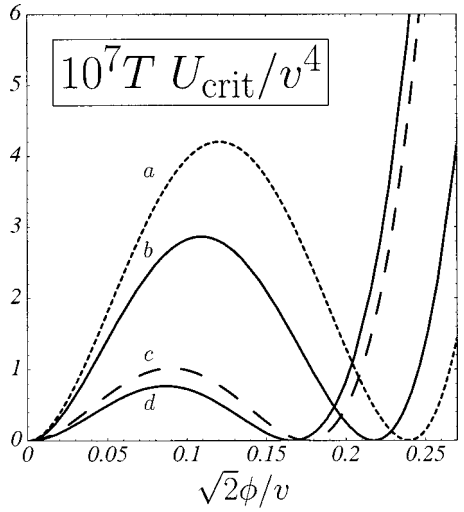


FIG. 9. The critical potential; comparison with perturbation theory (see text).

would lead to a dramatic decrease of the surface tension, up to several orders of magnitude. Finally, we consider the latent heat $L$, defined at the critical temperature as

$$L = T\left(\frac{dU(\bar{\rho}_0)}{dT} - \frac{dU(0)}{dT}\right)\Bigg|_{T=T_c}. \tag{5.4}$$

Using Eqs. (4.2), (4.3), and (3.5) we obtain

$$L = (m_H^2 - 2m_R^2)\bar{\rho}_0 + \frac{1}{2}\lambda_R T\bar{\rho}_0^2 + 3\Delta(\bar{\rho}_0) - \bar{\rho}_0\Delta'(\bar{\rho}_0). \tag{5.5}$$

The latent heat is related to the discontinuity and the mass of the scalar particle. Using Eq. (4.2), it can be shown that

$$L = \bar{\rho}_0 m_H^2, \tag{5.6}$$

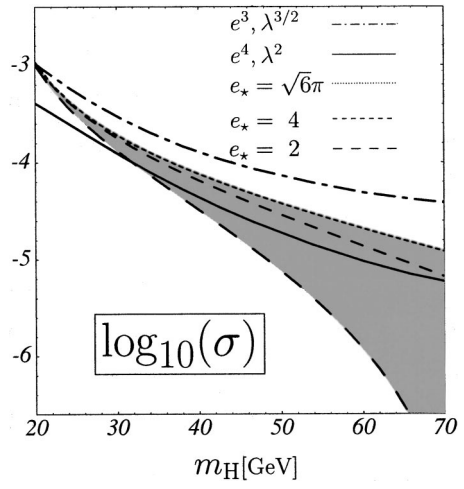


FIG. 10. The surface tension for various values of the Abelian fixed point in comparison with perturbation theory to order $(e^3,\lambda^{3/2})$ and $(e^4,\lambda^2)$.

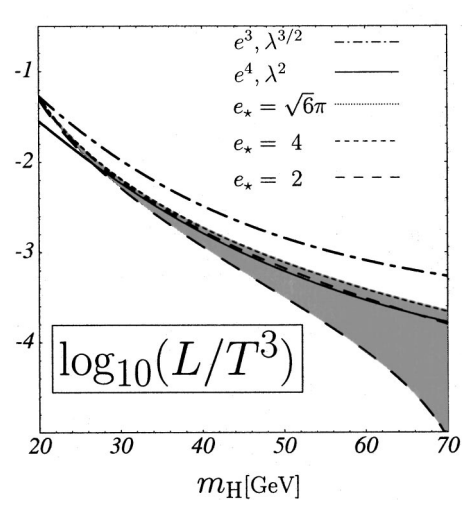


FIG. 11. The latent heat for various values of the Abelian fixed point in comparison with perturbation theory to order $(e^3,\lambda^{3/2})$ and $(e^4,\lambda^2)$.

which is also known as the Clausius-Clapeyron equation. This relation was shown to be fulfilled within an explicit gauge-invariant perturbative calculation [16]. However, it remains not true within standard perturbation theory; the perturbative values for the latent heat as found in Ref. [15] are all below the value given through the Clausius-Clapeyron relation (5.6). The deviation varies between a few percent up to 15–20 % for $m_H$ between 20 GeV and 70 GeV, and is larger at order $(e^4,\lambda^2)$ than at order $(e^3,\lambda^{3/2})$.

The latent heat in units of the critical temperature, is displayed in Fig. 11 for various values of the effective Abelian fixed point, and in comparison with perturbation theory to order $(e^3,\lambda^{3/2})$ and $(e^4,\lambda^2)$. The shaded region covers the interval $2 \leqslant e_\star \leqslant \sqrt{6}\pi$. We again observe a sharp decrease for small $e_\star$ and large Higgs boson mass as in Fig. 7. It is interesting to note that the curve for $e_\star = 4$ roughly agrees with the two-loop perturbative result for all $m_H$ above 30 GeV. This is not the case for the surface tension. Comparing Fig. 11 with Fig. 10, we notice that the effect of the running gauge coupling is more pronounced for the surface tension, because the entire region for $\bar{\rho} \leqslant \bar{\rho}_0$ enters Eq. (5.3), while the latent heat is only affected by $\bar{\rho}_0$.

### D. Characteristic scales

We discuss the results obtained so far in terms of the characteristic scales relevant for the phase transition. Most of the qualitative (and even quantitative) features can be understood once these scales are known.

In Fig. 12, we have depicted the relevant momentum scales as a function of the Higgs mass. The top line at $k = \Lambda$ corresponds to the scale of dimensional reduction, that is, the starting point of the flow in 3D. The scales $k_s$, $k_{\rm VEV}$, and $k_{\rm stable}$ (full lines) describe characteristics of the potential, the scale $k_{\rm cr}$ (dashed lines, for two values of the Abelian fixed point), the characteristics of the gauge sector, and $k_{\rm flat}$ (dashed-dotted line) the scale where scalar fluctuations can

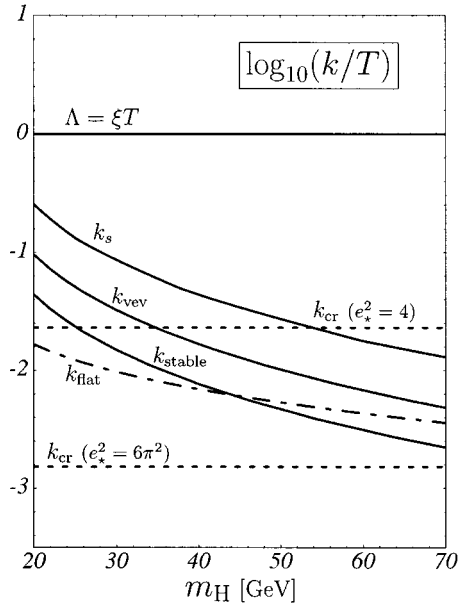


FIG. 12. Characteristic scales (see text).

no longer be neglected within the nonconvex part of the potential. All these scales are now discussed in detail.

At $k=k_s$, the origin of the effective potential stabilizes, $U'(\bar{\rho}=0)=0$, as the mass term squared at vanishing field changes sign. The free energy has two local minima for scales below $k_s$. This scale is therefore a good estimate for the scale of discontinuity. In Ref. [9], an estimate for this scale has been given, based on a local polynomial approximation for the potential. Within our conventions, it reads $k_{\rm dis}\approx 0.18e^4(T)/\lambda_R(T)$ for a sharp cutoff, and roughly coincides with $k_s$ as presented here ($k_{\rm dis}/k_s$ ranges between 1 to 3).

The scale $k\approx k_{\rm VEV}$ indicates when the VEV $\bar{\rho}_0$ is within 1% of its final value, eventually reached for $k\to 0$. However, this is not yet the scale where the critical potential has reached a stable shape, which actually happens only at about $k\approx k_{\rm stable}$. This results from the fact that the effective photon mass squared $2\bar{e}^2(k)\bar{\rho}$ (within the nonconvex part of the potential) is smaller than the photon mass at the minimum in the SSB regime (5.2), and the decoupling takes place only at smaller scales. Here, we have obtained $k_{\rm stable}$ comparing the depth of the potential $U(0)-U(\bar{\rho}_0)$ at $\bar{\rho}_0$ with the height of the barrier $U(\bar{\rho}_{\rm max})-U(0)$, demanding this ratio to be below $\approx$5%. At $k=k_{\rm stable}$, the VEV is as close as 0.1% to its final value.[14]

The crossover scale $k_{\rm cr}$ characterizes the crossover from the Gaussian to the Abelian fixed point. For $e_\star^2=6\pi^2$, we see that $k_{\rm cr}$ is about 1–2 orders of magnitude smaller than the scale $k_s$, which explains why the running gauge coupling has, in this case, only a small numerical effect on the properties of the phase transition. From the fact that the scales $k_{\rm VEV}$ and $k_{\rm stable}$ are separated by an order of magnitude ($k_{\rm VEV}/k_{\rm stable}\approx 5$), we can conclude that the running of the gauge coupling has a stronger effect on physical observables based on the entire effective potential (like the surface tension), than those related only to the VEV (such as the latent heat). This is quantitatively confirmed by the findings displayed in Figs. 6, 7, 10, and 11. For $e_\star^2=4$, we realize that the corresponding crossover scale is of the same order of magnitude as the scales $k_s$, $k_{\rm VEV}$, and $k_{\rm stable}$.[15] This is the region where the running of the gauge coupling has a strong quantitative effect on the properties of the phase transition, leading to a significant decrease of the strength of the transition.

Finally, we have also indicated the scale $k_{\rm flat}$ (dashed-dotted line), which is an estimate for the scale where the flattening of the inner part of the effective potential sets in. We obtained $k_{\rm flat}$ from solving $k^2+U_k'(\bar{\rho})\approx 0$ numerically for $k$ in the nonconvex part of the potential, with $U_k$ the leading-order solution for the free energy.[16]

In Ref. [13] an estimate for the ratio of $k_{\rm flat}/k_{\rm stable}$ has been obtained, based on an investigation of the surface tension of the 3D Abelian Higgs model in the universal limit $\Lambda\to\infty$. There it was found that $k_{\rm flat}^2/k_{\rm stable}^2\approx\bar{e}^2/M$, with $M$ being the 3D photon mass. The boundary $k_{\rm flat}^2/k_{\rm stable}^2\approx 1$ yields the relation $k_{\rm flat}\approx(e^2T/2\bar{\rho}_0)^{1/4}k_{\rm stable}$, which, using the data for $k_{\rm stable}$ as in Fig. 12, coincides within a few percent with the line for $k_{\rm flat}$ as obtained above. Corrections to the universal limit can be expanded as a series in $M^2/\Lambda^2$ [13]. In the present case, we start at a finite scale $\Lambda=\xi T$, but the smallness of $M^2/\Lambda^2$ (ranging from 0.2 to 0.001 for 20 GeV $\leqslant m_H\leqslant$70 GeV) is responsible for the small corrections with respect to the universal limit $\Lambda\to\infty$. Being close to the universal limit of the effective 3D theory also explains why the dependence on the matching parameter $\xi$ is rather small.

We now come back to the discussion of $k_{\rm flat}$ from Fig. 12, which, by definition, sets the scale below which the scalar fluctuations trigger the flattening within the nonconvex part of the potential, and hence the scale below which these fluctuations should no longer be neglected. First notice, that the scale of discontinuity $k_s$ is bigger than $k_{\rm flat}$ by an order of magnitude. We can thus expect that the scale of discontinuity is only weakly affected by the scalar fluctuations. Also, $k_{\rm VEV}>k_{\rm flat}$ by a factor of $\approx$5. Finally, for small Higgs field mass, $k_{\rm flat}$ is also smaller than $k_{\rm stable}$. In this region, only small quantitative changes are expected if the scalar fluctuations are taken into account. This is no longer the case for large Higgs field mass, where $k_{\rm flat}\geqslant k_{\rm stable}$. However, as these effects concern mainly the nonconvex part of the potential, and thus quantities like the surface tension, we can

[14]Remember that the critical potential at $k_{\rm stable}$, within the present approximations, is about the same as at $k=0$, as no substantial running takes place below $k_{\rm stable}$.

[15]In Fig. 12, the scales $k_s$, $k_{\rm VEV}$, $k_{\rm stable}$, and $k_{\rm flat}$ have been obtained for $e_\star^2=6\pi^2$. The corresponding results for $e_\star^2=4$ deviate (for larger Higgs boson mass) only slightly from the curves as presented here. This minor difference is of no relevance for the present discussion.

[16]A similar though slightly shifted curve for $k_{\rm flat}$ is obtained from solving $k^2+U_k'(\bar{\rho})+2\bar{\rho}U_k''(\bar{\rho})\approx 0$.

still expect that the latent heat and the VEV are only moderately affected.

These last observations are also relevant for the applicability of Langer's theory of bubble nucleation. The concept of an interface tension, as defined in Eq. (5.3), is based on the implicit assumption that the scale $k_{\rm stable}$ can indeed be identified. A criterion for this being the case is the smallness of the perturbative expansion parameter. From our consideration we can conclude that this will become more and more difficult for increasing $e^2 T_c/2\overline{\rho_0} \geqslant 1$, that is, for very weakly first-order phase transitions.[17]

### E. Higher-order corrections

Finally, we comment on the higher-order corrections, which are expected from operators neglected within the present approximation. Clearly, the results presented here are affected by the approximations performed, most notably through (i) the derivative expansion, (ii) neglecting the scalar field fluctuations as opposed to the gauge-field ones, (iii) approximating the infrared regime of the Abelian charge by an effective fixed point, and (iv) computing the initial conditions perturbatively. We discuss these approximations now one by one.

(i) The leading-order terms of the derivative expansion are known to correctly describe critical equations of state and scaling solutions for a variety of $O(N)$-symmetric scalar models in 3D. Although little is known about the convergence of such an expansion, it appears that the smallness of the anomalous dimensions controls the influence of higher-order derivative operators in the effective action. Therefore, an *a posteriori* consistency check for the reliability of the derivative expansion consists in computing the corresponding scalar and gauge-field anomalous dimensions $\eta_\varphi$ and $\eta_F$. In the present case, this involves more complicated higher-order threshold functions (for their definitions and further details, see Ref. [9]). At the scale $k \approx k_{\rm stable}$, we can compute the scalar anomalous dimension self-consistently from the explicit solution for the effective potential, obtained while neglecting $\eta_\varphi$. We find that $|\eta_\varphi| \leqslant 0.005$ in the interval considered, which is consistent with our initial approximation $\eta_\varphi = 0$ and justifies the derivative expansion within the scalar sector. For $N=1$, the gauge-field anomalous dimension $\eta_F$ can be estimated in a similar way. It becomes of order one only when the nontrivial fixed point is approached. We find that $\eta_F$ ranges from 0.03 to 0.4 within the range of Higgs field masses considered here and for $e^2_\star \approx 6\pi^2$. A main difference between the scalar and the gauge-field sector is that the gauge-field anomalous dimension grows large ($\eta_F = 1$) at a scaling solution. Therefore, one expects that higher-order corrections within a derivative expansion (or the momentum dependence of the gauge coupling) can become important at a scaling solution and should not be neglected. In the present case, however, the scales relevant for the first-order phase transition have been reached before the Abelian charge finally runs into its nontrivial fixed point, that is before $\eta_F = 1$. Therefore we can expect that the derivative expansion behaves reasonably well even for the gauge-field sector.

(ii) In the same way, we can check the validity of neglecting scalar fluctuations within the nonconvex part of the effective potential. It is found that the self-consistent inclusion of scalar fluctuations to leading-order, results in corrections to the order of a few percent, increasing with increasing Higgs field mass (see Appendix C). This agrees also with the discussion of the preceding section, where it was argued that scalar fluctuations should no longer be neglected as soon as $k_{\rm flat}$ is of the order of $k_{\rm stable}$. Clearly, the weaker the first-order phase transition the more scalar fluctuations will become relevant at the phase transition. For a quantitatively more reliable computation of thermodynamical quantities in the weakly type-I region, one has to go beyond the present approximation and include scalar fluctuations. All the present approximations can be improved in a systematic way, as has been emphasized earlier. This can be done either along the lines outlined in Sec. II E, or by a straightforward numerical integration of the flow equation as in Ref. [12].

(iii) The main uncertainty in the present understanding of the $U(1)$-Higgs theory is linked to the gauge sector of the theory, i.e., the precise infrared behavior of the Abelian gauge coupling. Here we have effectively parametrized this uncertainty in terms of an Abelian fixed point motivated by previous work based on large-$N$ extrapolations and Wilsonian RG techniques. A precise determination of the correct fixed point requires the study of the momentum and of the field dependence of the Abelian charge. Our approximation assumes that the field gradients of the function $e^2_\star(k,\overline{\rho})$ remain sufficiently small within the nonconvex part of the potential at scales above $k \approx k_{\rm stop}$. In the large-$N$ limit, where this fixed point is well understood, the results in the present approximation are in very good agreement with the result found within a fixed dimension computation.

(iv) The points (i)–(iii) concerned the approximations on the level of the flow equation. These are the most important ones, because they act back on $\Gamma_k$ upon integration of the flow. An additional approximation concerns the initial conditions to the flow. Here, they have been obtained from the dimensional reduction scenario within a perturbative loop computation. For the present purposes, it was sufficient to use a one-loop perturbative matching as given in Sec. III, although the two-loop matching has been reported as well [30]. These higher-order effects can be taken into account in principle; in practice, this will not be necessary because their quantitative influence is smaller than the contributions from the scalar fluctuations for larger Higgs field mass, which have already been neglected. In any case, a small change of the initial condition cannot change the main effect reported here. Except for small Higgs field masses, the dominant contributions come from integrating-out modes in 3D. This follows directly from Fig. 5, which shows that the main running of the VEV takes place below the scale of dimensional reduction.

Finally, we remark that the quality of a given approximation can also be assessed by studying the dependence on the

[17] The treatment of very weakly first-order transitions based on coarse-grained potentials has been considered in Ref. [31].

coarse-graining scheme. This discussion will be the subject of the following section.

## VI. SCHEME DEPENDENCE

All quantitative results present up to now have been obtained for a sharp cutoff regulator. It is a straightforward consequence of the Wilsonian renormalization-group approach that physical observables obtained from a solution to a Wilsonian flow equation, will not depend on the precise form of the coarse graining. Unfortunately, this conclusion holds only if the *full* effective action is computed. On a technical level, this is barely possible, and truncations of the effective action have to be employed. It is precisely this truncation that can introduce a spurious coarse-graining scheme dependence for physical observables. In this section we address the question to what extent the physical observables, as obtained in the preceding section, do (or do not) depend on the precise form of the coarse graining. In doing so, we are able to present quantitative ''error bars'' related to the scheme dependence. We also present evidence for an intimate quantitative link between the scheme dependence and the truncations employed.

### A. Scheme dependence vs truncations

Consider the case of computing some physical observable from the solution to a (truncated) Wilsonian flow. It goes without saying that a *strong* dependence of this observable on the coarse graining employed is not acceptable as it would cast serious doubts on the truncations performed so far. With ''strong'' we mean ''inducing large quantitative,'' or even ''qualitative'' changes. On the other hand, a *weak* scheme dependence of certain physical observables is a sign for the viability of the approximation employed. In fact, if we were able to solve the flow equations without truncating the effective action $\Gamma_k$, the final result in the physical limit $k\to 0$, which is by construction nothing else but the full quantum effective action $\Gamma$, should not depend on the details of the particular coarse graining employed. There is little hope for this holding true for any truncation of the effective action $\Gamma_k$ as any truncation necessarily neglects infinitely many operators.

The coarse-graining procedure is implemented through the momentum-dependent operator $R_k(q^2)$. It couples to all the operators present in $\Gamma_k$ in a well-defined way, that is, according to the flow equation (2.1). Replacing a coarse graining by another coarse graining, implies that the effective coupling of $R_k(q^2)$ to the operators contained in the effective action, changes accordingly. A truncation of the effective action amounts to neglecting infinitely many operators to which the coarse graining, in principle, is sensitive. Therefore, studying the scheme dependence will probe whether some relevant operators (for the problem under investigation) have been neglected, or not. In this light, the indirect feedback of some relevant operators should manifest itself through some strong eigenmode with respect to a change of the coarse-graining procedure.

Although these arguments, as presented so far, are of a purely qualitative nature, we will show in the sequel that they can indeed be given a quantitative meaning.

### B. Coarse grainings

Before studying in detail the scheme dependence of our results, we will briefly review the main requirements for a viable coarse-graining procedure. There are basically three key points to be considered. The first one concerns the possible zero modes of the propagators, which typically cause strong infrared problems within perturbative loop expansions in $d<4$ dimensions. These are properly regularized, if

$$\lim_{q^2\to 0} R_k(q^2)>0 \tag{6.1a}$$

holds true. In this way, the effective inverse propagator for a massless mode reads $q^2+R_k(q^2)$, and has a well-defined infrared limit. The second point concerns the infrared limit of the effective action $\Gamma_k$, which should coincide with the usual effective action for $k\to 0$. This is the case, if

$$\lim_{k\to 0} R_k(q^2)=0. \tag{6.1b}$$

Finally, we have to make sure that the correct initial effective action in the ultraviolet limit is approached, which is guaranteed by

$$\lim_{k\to\infty} R_k(q^2)\to\infty. \tag{6.1c}$$

Any function $R_k(q^2)$ with the above properties, can be considered as a coarse graining [5,13]. It is convenient to rewrite $R_k$ in terms of dimensionless functions $r(q^2/k^2)$ as

$$R_k(q)=Zq^2 r(q^2/k^2), \tag{6.2}$$

where $Z$ corresponds to a possible wave-function renormalization ($Z_\phi=1$ in our approximation).

Let us introduce two classes of regulator functions, which are commonly used in the literature. The first one is a class of *powerlike* regularization schemes given by the coarse-graining function

$$\Upsilon_p(y)=y^{-n}, \tag{6.3}$$

and $y\equiv q^2/k^2$. The particular case $n=1$, corresponds to a masslike regulator $R_k\sim k^2$, and $n=2$ to a quartic regulator $R_k\sim k^4/q^2$. These algebraic regulators are often used because the related threshold functions can be computed analytically. On the other hand, these regulators decay only algebraically for large momenta, which can, in principle, lead to an insufficiency in the integrating out of the hard UV modes.

A second convenient class of regulators consists of exponential ones, parametrized as

$$r_e(y)=\frac{1}{\exp(cy^n)-1}, \tag{6.4}$$

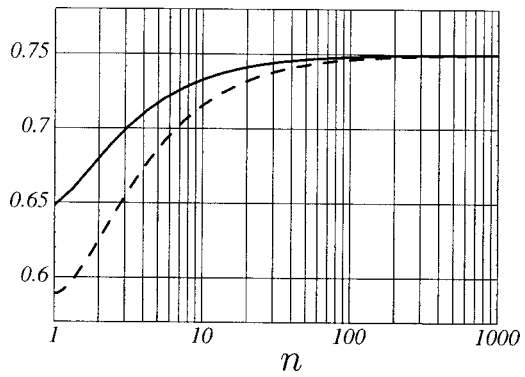


FIG. 13. The expansion coefficient $a_1$ (see text).

where $c$ is a constant. The exponential regulator with $n=c=1$, has been used previously in various numerical investigations [9,10,27]. The suppression of large momentum modes $q^2 \gg k^2$ to the flow, is now exponential and thus much stronger than in the case of algebraic regulators. It is expected that this property is at the basis for a good convergence of approximate solutions.

Both classes of regulator functions depend on the parameter $n$, with $1 \leqslant n \leqslant \infty$. In the limit $n \to \infty$, they both approach what is known as the sharp cutoff regulator, given by [3,4]

$$r_s(y) = \frac{1}{\theta(y-1)} - 1. \tag{6.5}$$

We will now consider the dependence of certain physical observables on particular choices of these regulators.

### C. Tricritical point and large-*N* limit

We have given an estimate for the endpoint of the critical line in Eq. (4.5). Its mere existence is closely linked to the presence of an Abelian fixed point, although it will be within the domain of validity only for small values of the latter. Both functions $F_1$ and $F_2$ depend explicitly on the RS, and so does the solution to Eq. (4.2). In the general case, the endpoint of the critical line also depends on the RS. Instead of Eq. (4.5), which is the result for a sharp cutoff, we find for the general case

$$\frac{m_H^2}{M^2} = \frac{8a_1}{3\pi^2} e_\star^2, \tag{6.6}$$

where terms $\mathcal{O}(e)$ have been dropped. The entire scheme dependence is now encoded in the coefficient $a_1$, given by

$$a_1 = -\frac{3}{2} \int_0^\infty dy \, \frac{r'(y) y^{-1/2}}{[1+r(y)]^3} \tag{6.7}$$

in $d=3$ dimensions. This coefficient belongs to a set of expansion coefficients $a_k$ characterizing a coarse-graining scheme (see Appendix A for their general definition and more details). For each of the two classes of regulators, the coefficient $a_1$ can be calculated as a function of the parameter $n$. In Fig. 13, the dashed line corresponds to the powerlike, and the full line to the exponential regulator class with $c=\ln 2$. For this choice of $c$, both sets of regulators are normalized to $r(1)=1$. For a powerlike regulator, we find explicitly $a_1 = \frac{3}{4}\Gamma[1+1/2n]\Gamma[2-1/2n]$, and for the exponential one $a_1 = \frac{3}{8} n^{-1} c^{1/2n} (2^{1/2n}-2)\Gamma[-1/2n]$. It is interesting to note that although these classes of regulators do have strong qualitative differences, the coefficient $a_1$, which only involves a folding of $r(y)$ over all momenta, is rather stable (i.e., $\pm 10\%$ about the mean value).

We shall compare the numerical value of the tricritical point with results obtained in the large-$N$ limit via the $\epsilon$ expansion [32] or a fixed dimension computation in $(d=3)$ [33]. As argued in Sec. II B, the Abelian fixed point reads $e_\star^2 = 6\pi^2/N$ in the large-$N$ limit, and our above result therefore becomes

$$\frac{\lambda_3}{e_3^2} = 16 a_1 \frac{1}{N} \approx (9.4 - 12.0) \frac{1}{N}. \tag{6.8}$$

The $\epsilon$ expansion, to leading order, yields

$$\frac{\lambda_3}{e_3^2} = (54 - 136\epsilon) \frac{1}{N}. \tag{6.9}$$

This is to be compared to the result of Ref. [33], which reads

$$\frac{\lambda_3}{e_3^2} = \frac{96}{\pi^2} \frac{1}{N} \approx 9.9 \frac{1}{N}. \tag{6.10}$$

While Eq. (6.9) fails to give a reliable answer at $\epsilon = 1$, we observe that our result (6.8) is in good numerical agreement with Eq. (6.10).

### D. Scheme dependence of the critical potential

Here, we consider the task of computing the critical potential for coarse grainings other than the sharp cutoff. First, we have to obtain the corresponding fluctuation integrals. The most general expression (for arbitrary scheme) has been given in Appendix B. This expression still contains an integral over momenta to be performed, which is how the scheme dependence enters into the expression for the fluctuation integral $\Delta_k$. Then, the criticality conditions (4.2) have to be solved to find $T_c$ and $\overline{\rho_0}$. The sharp cutoff allowed an analytical computation of $\Delta_k$, (B.5), and thus of the functions $F_{1,2}$ in Eq. (4.3).

Below, in addition to the sharp cutoff, we consider the classes of powerlike regulators (6.3) and exponential regulators (6.4). From the powerlike regulators, we consider the limiting cases $n=1$ (i.e., a masslike regulator $R_k = k^2$) and $n=\infty$ (the sharp cutoff). As an intermediate case we consider also the case $n=2$ (i.e., the quartic regulator $R_k = k^4/q^2$). The exponential regulators are represented for $n=1$ [i.e., $R_k = q^2/(\exp q^2/k^2 - 1)$], and $n=\infty$ (the sharp cutoff). A continuity argument suggests that the critical potentials for intermediate values of the coarse-graining parameter $n$ should appear within those limits set by $n=1,2$ and $n=\infty$.

No explicit analytical expressions for the coarse-grained free energy have been found in these cases. For the masslike and the quartic regulator we used the integrals (B7) and (B8),

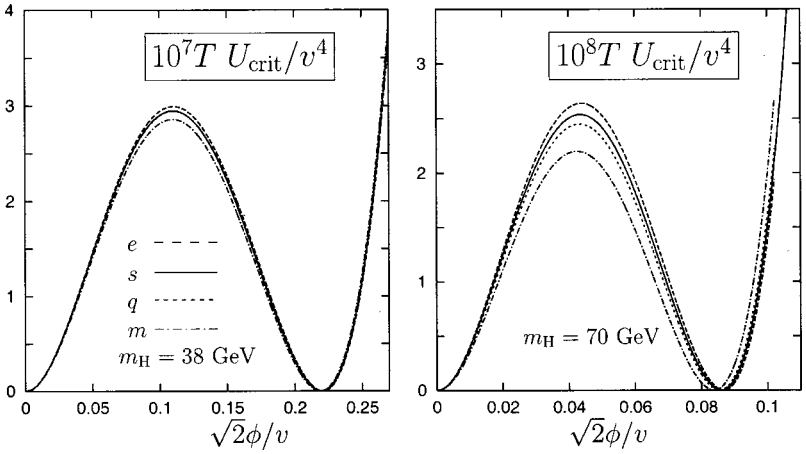


FIG. 14. The critical potential for $m_H = 38$ GeV (left panel) and $m_H = 70$ GeV (right panel), and different regulator schemes: exponential regulator (*e*), sharp cutoff (*s*), quartic regulator (*q*), and masslike regulator (*m*).

respectively, while Eq. (B2) is used for the exponential regulator. Then, the problem of solving the criticality conditions reduces to the optimization of two integral equations.

We find that the critical temperature $T_c$, depends very weakly on the different schemes. Indeed, plotting $T_c$ as a function of the Higgs field mass, we find that the lines corresponding to different schemes are almost on top of each other, inducing a relative error well below the 1% level (and thus below the error already present due to other approximations). A similar situation holds for the VEV, where we find a relative error below a few percent.

In Fig. 14, the entire critical potential (in units of the 4D VEV) is displayed for different coarse grainings at $m_H = 38$ GeV (left panel) and at $m_H = 70$ GeV (right panel). The labels *s*, *q*, *m*, and *e* denote, respectively, the sharp cutoff, the *q*uartic/*m*asslike regulator, and the exponential cutoff from Eq. (6.4) for $n=1$ and $c=1$.

We first consider $m_H = 38$ GeV, and notice that the *s* and *q* lines turn out to be on top of each other. Furthermore, it is realized that the VEV is nearly independent of the RS, as is the shape of the potential close to the minima. The main dependence concerns the local maximum of the critical potential. This dependence will therefore affect integrated quantities like the surface tension, but not those related to the VEV, such as the latent heat. The error for the surface tension in the present case is a few percent.

For $m_H = 70$ GeV, the dependence on the scheme is more pronounced than in the previous case. Furthermore, the VEV receives—for the masslike regulator—a sizable shift towards smaller values. Again, the variance is strongest around the maximum of the critical potential, and dominant in the nonconvex region of the critical potential. The additional shift in the value of the VEV entails a corresponding shift for the outer region of the effective potential, as opposed to the case for smaller Higgs field mass.

It is interesting to make contact with the qualitative considerations presented at the beginning of this section, and to compare the scheme dependence observed in Fig. 14 with the reliability of the coarse-grained potential in its different regions, due to the approximations employed. Recall that the present computation is based on neglecting the scalar fluctuations. This approximation is more reliable for the outer part of the potential than for the nonconvex part of it (more precisely, around a small region of the maximum of the inner part of the potential). Here, scalar fluctuations ultimately cause the flattening of the potential in the IR limit. While we have seen in Sec. V D that this approximation is still reliable for $m_H = 38$ GeV, we certainly expect larger corrections for $m_H = 70$ GeV (see the discussion of Secs. V D and V E). It is quite remarkable that the scheme dependence indeed seems to reflect the weakness of the approximation for this region of the potential. Our computation thus turns the qualitative statement into a quantitative one.

Finally, we briefly comment on the different regulators used. It is well-known that the masslike regulator is marginal in the sense that it has a poor UV behavior, which makes its use for certain applications questionable (a more refined discussion has been given in Ref. [22]). From Fig. 14, we learn that the critical potential as obtained for the masslike regulator, deviates the most from the results for the other regulators employed. Considering the class of powerlike regulators, we see from Fig. 14 that the width between the quartic and the sharp cutoff limit is significantly smaller than the deviation for the masslike regulator. This observation strongly suggests that the masslike regulator should be discarded for quantitative considerations, although it remains, in the present example, a useful regulator for studying the main qualitative features of the problem.[18] Discarding the masslike regulator from our discussion, we end up with the observation that the error induced through the scheme dependence is of the same order of magnitude for algebraic as for exponential regulators. For the present case, and at this level of accuracy, no further qualitative differences are observed between the exponential regulators (6.4) and the powerlike ones (6.3) for $n \geqslant 2$.

In summary, we conclude that a quantitative analysis of the scheme dependence indeed yields nontrivial information regarding the accuracy of the approximations or truncations employed, as suggested by the qualitative argument presented in Sec. VI A. In addition, we have found some evidence for why a masslike regulator, as opposed to exponen-

[18]This conclusion coincides with those of Ref. [22] based on more formal considerations regarding masslike regulators.

tial or higher-order powerlike regulators, should be discarded for accurate quantitative considerations. However, as the qualitative features are still well described by a masslike regulator, and as the quantitative deviation is not too big, this also suggests that a mass term regulator could be very useful for an error estimate.[19] Typically, analytical computations are largely simplified for masslike regulators, allowing for a simple cross check of the results.

## VII. SUMMARY AND OUTLOOK

We have studied, in detail, the first-order phase transition of Abelian Higgs models in $3+1$ dimensions at finite temperature. Properties of the transition are determined by the underlying fixed-point structure of the 3D theory, such as the crossover of the Abelian charge from the Gaussian to the Abelian fixed point. We computed all physical observables at the phase transition, the phase diagram in the domain of first-order transitions, and the tricritical point. The analysis has been restricted to the region of parameter space, where the dimensional reduction scenario applies, and a perturbative matching of the 4D parameters to the corresponding 3D ones, is possible. The main contribution to the free energy (and thus to the physical observables at criticality) stem from the remaining effective 3D running, for which we have used a Wilsonian renormalization group to leading order in the derivative expansion, neglecting the scalar, but not the gauge-field anomalous dimension. The latter is related to the nontrivial running of the Abelian gauge coupling, which is described by an effective fixed point. While this fixed point is well understood in the large-$N$ limit, where the tricritical fixed point is known, its precise form is not yet established for the relevant case of $N=1$. We therefore studied the parametric dependence of physical observables on the fixed-point value. A quantitative discussion of the relevant physical scales, which are easily accessible within a Wilsonian framework, has also been given.

The main effect on physical observables due to the presence of a nontrivial fixed point, depends on the ratio between the crossover scale $k_{\rm cr}$ (which defines the crossover to the Abelian fixed point) and the typical scales characterizing the first-order phase transition (like the discontinuity scale $k_{\rm dis}$, or $k_{\rm stable}$). For $k_{\rm cr}$ small as compared to $k_{\rm stable}$, the observed dependence is weak. The sizable deviations from the perturbative $\bar{e}^2(k)\approx\bar{e}^2(\Lambda)$ behavior only set in at very small scales below $k_{\rm stable}$, and are no longer relevant for the phase transition itself in this situation. The main effects are restricted to alterations in the far infrared region, like the details of the flattening of the inner part of the potential. On the other hand, a strong dependence emerges for $k_{\rm cr}$ larger than $k_{\rm stable}$.

Most of our results for the physical observables can be summarized as in Fig. 15. Here, the reference values $T_{\rm ref}$ and $\bar{\rho}_{\rm ref}$ are given for $e_\star=\sqrt{6}\pi$ (which corresponds roughly to $k_{\rm cr}\approx k_{\rm stable}$), and for the sharp cutoff regulator. In the present

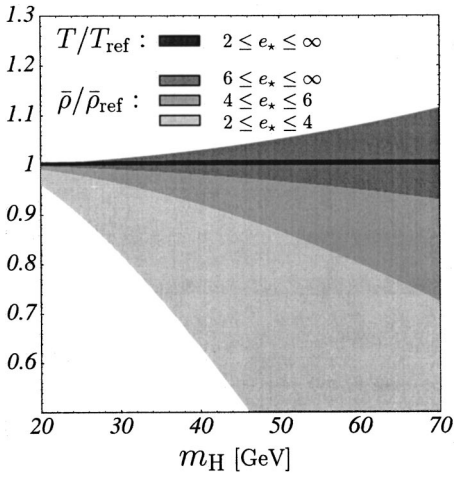


FIG. 15. The relative variation of $T_c$ and $\bar{\rho}_0$ with the effective Abelian fixed point. Here, the regions $T/T_{\rm ref}$ and $\bar{\rho}/\bar{\rho}_{\rm ref}$ compare the critical temperature and the VEV as a function of $e_\star$. The reference values are obtained for $e_\star=\sqrt{6}\pi\approx 7.7$.

approximation, the critical temperature is insensitive to the running gauge coupling. On the other hand, the VEV appears to be quite sensitive to the actual fixed point value, in particular for larger Higgs field mass. The phase transition weakens significantly for small fixed-point values. The reason is that the gauge coupling is decreasing strongly for small fixed-point values at scales larger than the scale where the critical potential reaches its degenerate shape, that is above the scale of decoupling. These results compare well with perturbation theory, except for very large or very small values for the Abelian fixed point. Corrections due to the nontrivial scaling of $\bar{e}^2(k)$, remain below 10% for $e_\star^2 > 6\pi^2$ and $m_H$ below 70 GeV, but do grow large as soon as $e_\star^2$ is below $6\pi^2$. We conclude that $e_\star^2\approx 6\pi^2$ is a good leading-order approximation for a small Higgs field mass as higher-order corrections are small. For $m_H=30$ GeV, we also compared the value for the critical temperature with lattice simulations and found agreement below 4%. The sensitivity on $e_\star^2<6\pi^2$ for larger Higgs mass, in turn, requires a better determination of the fixed point in this domain. This concerns, in particular, physical observables like the critical exponents at the endpoint of the line of first-order phase transitions.

For a generic regulator function the free energy in the type-I regime has been given as an integral (one remaining integration). For the case of a sharp cutoff regulator, we obtained an explicit analytical solution for the free energy, given the nontrivial scale dependence of the Abelian charge. In the present paper, we evaluated all relevant quantities for initial conditions obtained from a perturbative dimensional reduction scenario relevant for a high-temperature (cosmological) phase transition.

The explicit result for the effective potential can also be of use for applications to the superconducting phase transition, or for the nematic to smectic-A phase transition in certain liquid crystals. The main change would concern the initial potential for the effective 3D flow of the potential, and the numerical value of the Abelian charge at that scale.

[19] An error estimate based on the masslike regulator is rather conservative as it seems to overestimate the scheme dependence.

These changes affect, in particular, the ratio $k_{\rm cr}/k_{\rm stable}$, and, therefore, the above discussion, as both scales depend in a qualitatively different manner on $e^2(\Lambda)$ and $U_\Lambda$.

In addition, we studied the dependence of our results on the coarse-graining procedure employed. We have seen that the physical observables do depend only very weakly on the coarse graining. This is encouraging, as a strong dependence would have cast serious doubts on the approximations used. Furthermore, we employed a variety of qualitatively different coarse grainings ranging from the masslike and other polynomial regulators over exponential ones to the sharp cutoff regulator. Therefore, our result can be seen as an important consistency check of the method. The weak variation, with respect to the coarse graining, which is to be interpreted as an ''error bar'' for the observables, is smaller or of about the same size as the error expected from higher-order operators for the coarse grainings studied. This error bar would vanish only if no truncation to the effective action would have to be performed. We also observed an intimate relationship between the truncation of the effective action, and the error bar introduced through the scheme dependence. More precisely, it is observed that the scheme dependence is largest in regions where a similarly large effect, due to the neglecting of the scalar fluctuations in the nonconvex region of the potential, is expected. While this result is not entirely unexpected, a quantitative evidence for it has never been presented before. It would be useful if further quantitative results in this direction could be established. This concerns, in particular, the cross dependencies between an optimal coarse graining that minimizes the scheme dependence, and an optimized convergence of systematic truncations and approximations [34].

An important open question for future work concerns the precise IR behavior of the Abelian charge. This, of course, is an intrinsic problem of the 3D theory. As argued, our current understanding is mainly limited due to an insufficient understanding of the field and/or momentum dependence of the Abelian charge. It might be fruitful to consider alternatively a thermal renormalization group to improve the situation [24]. At the same time, the inclusion of higher-order corrections due to scalar fluctuations will also become important—close to the critical points—for a reliable determination of critical exponents and other universal quantities. It would also be interesting to consider the $SU(2)$-Higgs theory, where a nontrivial endpoint of the line of first-order phase transitions has been established recently. A field theoretical understanding of this endpoint is still missing, and a derivation of the related critical indices from field theory would be desirable. Again, one expects that the IR behavior of the gauge coupling, in competition with the scalar fluctuations, is responsible for the existence of the endpoint.

## APPENDIX A: REGULARIZATION SCHEME DEPENDENCE AND THRESHOLD FUNCTIONS

The solution of the flow equation (and the related physical observables) can be written as momentum integrals over a measure, which depends on the precise implementation of the coarse graining. We employ the notation of Ref. [13], where a scheme dependent measure has been given (in $d$ dimensions) as

$$I_r[f]=-\frac{d}{2}\int_0^\infty dy\,\frac{r'(y)}{[1+r(y)]^{1+d/2}}f(y) \tag{A1}$$

for momentum-dependent functions $f(y)$, where $y=q^2/k^2$, and $q$ is the loop momenta. As a consequence of the conditions (6.1) on the regularization function $r(y)$, it follows that the momentum measure $-r'(y)/(1+r)^{1+d/2}$ is peaked. The measure is normalized to one,

$$I_r[1]=1. \tag{A2}$$

This implies that $I_r[f]$ depends on the coarse graining as soon as $f$ displays a nontrivial dependence on momenta.

As an example, let's consider the threshold functions $l_n^d(\omega)$, defined as

$$l_n^d(\omega)=-(\delta_{n,0}+n)\int_0^\infty dy\,\frac{r'(y)y^{1+d/2}}{[y(1+r)+\omega]^{n+1}}. \tag{A3}$$

They are related to the above measure through

$$l_n^d(\omega)=\frac{2}{d}(\delta_{n,0}+n)I_r\left[\frac{P^{d+2}}{(P^2+\omega)^{n+1}}\right]. \tag{A4}$$

Here, we also introduced the dimensionless effective (regularized) inverse propagator

$$P^2(y)=y+yr(y). \tag{A5}$$

The threshold functions can always be expanded as a Taylor series in powers of $\omega$. Let us define the corresponding RS dependent expansion coefficients

$$a_k=I_r[P^{-k}]. \tag{A6}$$

which are the $k$th moments of $1/P$ with respect to the measure $I_r$. These coefficients appear in the computation of the endpoint of the critical line (6.6), which is proportional to the coefficient $a_1$. For a powerlike regulator $r(y)=y^{-n}$ [see Eq. (6.3)] we find for arbitrary dimension $d$

$$a_k=\frac{d}{2}\Gamma\left[1+\frac{k}{2n}\right]\frac{\Gamma\left[\frac{d}{2}+\frac{k}{2}\left(1-\frac{1}{n}\right)\right]}{\Gamma\left[1+\frac{d}{2}+\frac{k}{2}\right]}. \tag{A7}$$

A more detailed discussion of these coefficients and a related discussion of the convergence of amplitude expansions and optimized coarse-graining parameters, is given in Ref. [34].

### APPENDIX B: THE FLUCTUATION INTEGRAL

The fluctuation integral reads

$$\Delta_k(\overline{\rho}) = -\frac{1}{2\pi^2}\int_k^\Lambda d\overline{k}\int_0^\infty dy\,\frac{\overline{k}^2}{P^2}\,\frac{2e_\star^2\overline{\rho}r'(y)y^{5/2}}{2e_\star^2\overline{\rho}+P^2\overline{k}(1+\overline{k}/k_{\rm cr})}. \tag{B1}$$

Note that we have normalized $\Delta(0)=0$ in the above definition. The remaining integrals in Eq. (B1) can be solved in different ways, either first performing the momentum integration or the scale integration. Integrating first with respect to $\overline{k}$ yields (for the notation see Appendix A)

$$\Delta_k(\overline{\rho}) = I_r[\mathcal{U}(\overline{\rho},P)], \tag{B2}$$

where

$$\begin{aligned}3\pi^2\mathcal{U}(\overline{\rho},P) &= 2e_\star^2\overline{\rho}\int_k^\Lambda d\overline{k}\frac{P^3\overline{k}^2}{P^2\overline{k}(1+\overline{k}/k_{\rm cr})+2e_\star^2\overline{\rho}}\\ &= -2e_\star^2\overline{\rho}Pk_{\rm cr}(k-\Lambda)\\ &\quad + e_\star^2\overline{\rho}Pk_{\rm cr}^2\ln\left(\frac{2e_\star^2\overline{\rho}/P^2+k+k^2/k_{\rm cr}}{2e_\star^2\overline{\rho}/P^2+\Lambda+\Lambda^2/k_{\rm cr}}\right)\\ &\quad + 2e_\star^2\overline{\rho}Pk_{\rm cr}(4e_\star^2\overline{\rho}/P^2-k_{\rm cr})\\ &\quad \times G_{k,\Lambda}\left(1-\frac{8e_\star^2\overline{\rho}}{P^2k_{\rm cr}}\right),\end{aligned} \tag{B3}$$

with $I_r$ defined in Eq. (A1) and $P(y)$ in Eq. (A5). The function $G(\Omega)$ reads

$$G_{k,\Lambda}(\Omega) = \begin{cases} \dfrac{1}{2\sqrt{\Omega}}\ln\left(\dfrac{1+2k/k_{\rm cr}-\sqrt{\Omega}}{1+2k/k_{\rm cr}+\sqrt{\Omega}}\,\dfrac{1+2\Lambda/k_{\rm cr}+\sqrt{\Omega}}{1+2\Lambda/k_{\rm cr}-\sqrt{\Omega}}\right) & \text{for } \Omega>0,\\ \dfrac{-1}{\sqrt{-\Omega}}\left[\arctan\left(\dfrac{\sqrt{-\Omega}}{1+2k/k_{\rm cr}}\right)-\arctan\left(\dfrac{\sqrt{-\Omega}}{1+2\Lambda/k_{\rm cr}}\right)\right] & \text{for } \Omega<0,\\ \dfrac{2k_{\rm cr}(k-\Lambda)}{(k_{\rm cr}+2k)(k_{\rm cr}+2\Lambda)} & \text{for } \Omega=0.\end{cases} \tag{B4}$$

For a sharp cutoff regulator (6.5), the remaining momentum integration can be performed analytically to give

$$\begin{aligned}2\pi^2\Delta_k^{(s)} &= \frac{1}{3}\Lambda^3\ln\left(1+\frac{2e_\star^2\overline{\rho}k_{\rm cr}}{\Lambda(\Lambda+k_{\rm cr})}\right)-\frac{1}{3}k^3\ln\left(1+\frac{2e_\star^2\overline{\rho}k_{\rm cr}}{k(k+k_{\rm cr})}\right)-\frac{1}{3}k_{\rm cr}^3\ln\left(\frac{\Lambda+k_{\rm cr}}{k+k_{\rm cr}}\right)\\ &\quad +\frac{1}{6}(k_{\rm cr}^3-6e_\star^2\overline{\rho}k_{\rm cr}^2)\ln\left(\frac{\Lambda(\Lambda+k_{\rm cr})+2e_\star^2\overline{\rho}k_{\rm cr}}{k(k+k_{\rm cr})+2e_\star^2\overline{\rho}k_{\rm cr}}\right)+\frac{4}{3}e_\star^2\overline{\rho}k_{\rm cr}(\Lambda-k)\\ &\quad -\frac{1}{3}k_{\rm cr}(-16e_\star^4\overline{\rho}^2+10e_\star^2\overline{\rho}k_{\rm cr}-k_{\rm cr}^2)G_{k,\Lambda}(1-8e_\star^2\overline{\rho}/k_{\rm cr}).\end{aligned} \tag{B5}$$

We have normalized $\Delta(\overline{\rho})$ such that $\Delta(0)=0$.

On the other hand, performing first the scheme dependent momentum integration leaves us with the following remaining integrals:

$$\Delta^{(s)}(\overline{\rho}) = \frac{1}{2\pi^2}\int_k^\Lambda d\overline{k}\overline{k}^2\ln\left(1+\frac{2e_\star^2\overline{\rho}}{\overline{k}(1+\overline{k}/k_{\rm cr})}\right), \tag{B6}$$

$$\Delta^{(m)}(\overline{\rho}) = \frac{1}{2\pi}\int_k^\Lambda d\overline{k}\overline{k}^2\left(\sqrt{1+\frac{2e_\star^2\overline{\rho}}{\overline{k}(1+\overline{k}/k_{\rm cr})}}-1\right), \tag{B7}$$

$$\Delta^{(q)}(\overline{\rho}) = \frac{1}{2\pi}\int_k^\Lambda d\overline{k}\overline{k}^2\left[1-\left(1+\frac{e_\star^2\overline{\rho}}{\overline{k}(1+\overline{k}/k_{\rm cr})}\right)^{-1/2}\right]. \tag{B8}$$

Here, the indices refer to the sharp $(s)$, the masslike $(m)$, and the quartic $(q)$ cutoff function, as defined in Sec. VI.

### APPENDIX C: INCLUDING SCALAR FLUCTUATIONS

In order to obtain an estimate of the effect of the scalar fluctuations, we will solve Eq. (2.9) with $U_k$ on the right-

hand side, replaced by $U_\Lambda$, for a sharp cutoff regulator. The flow equation becomes

$$4\pi^2\frac{dU_k(\overline{\rho})}{k^2dk}=l_0^3\left(\frac{m_{1,\Lambda}^2(\overline{\rho})}{k^2}\right)+l_0^3\left(\frac{m_{2,\Lambda}^2(\overline{\rho})}{k^2}\right)+2l_0^3\left(\frac{2\overline{e}_3^2(k)\overline{\rho}}{k^2}\right), \tag{C1}$$

with the masses $m_i^2$ given through

$$m_1^2(\overline{\rho})=m_R^2+\overline{\lambda}_R\overline{\rho},\quad m_2^2(\overline{\rho})=m_R^2+3\overline{\lambda}_R\overline{\rho}. \tag{C2}$$

We introduce the functions

$$K(m^2)=-\frac{1}{4\pi^2}\int_\Lambda^k dy y^2\ln\left(1+\frac{m^2}{y^2}\right)=-\frac{1}{12\pi^2}\left[2m^2k-2m^3\arctan\left(\frac{k}{m}\right)+k^3\ln\left(1+\frac{m^2}{k^2}\right)-(k\leftrightarrow\Lambda)\right], \tag{C3}$$

$$J_i(\overline{\rho})=K[m_i^2(\overline{\rho})]-K[m_i^2(0)]. \tag{C4}$$

The solution to the flow (C1) then obtains, using also $\Delta^{(s)}$ from Eq. (B5), as

$$U_k(\overline{\rho})=U_\Lambda(\overline{\rho})+\Delta^{(s)}(\overline{\rho})+J_1(\overline{\rho})+J_2(\overline{\rho}). \tag{C5}$$

The effect of the additional terms on the shape of the critical potential is about a few percent, increasing towards higher values for $m_H$.


[1] B. I. Halperin, T. C. Lubensky, and S. Ma, Phys. Rev. Lett. **32**, 292 (1974); H. Kleinert, *Gauge Fields in Condensed Matter* (World Scientific, Singapore, 1989).
[2] P. G. de Gennes and J. Prost, *The Physics of Liquid Crystals* (Cambridge University, Cambridge, England, 1993).
[3] F. J. Wegner and A. Houghton, Phys. Rev. A **8**, 401 (1973); K. G. Wilson and I. G. Kogut, Phys. Rep. **12**, 75 (1974).
[4] J. Polchinski, Nucl. Phys. **B231**, 269 (1984).
[5] C. Wetterich, Nucl. Phys. **B352**, 529 (1991); Phys. Lett. B **301**, 90 (1993); Z. Phys. C **57**, 451 (1993).
[6] M. Reuter and C. Wetterich, Nucl. Phys. **B391**, 147 (1993); **B408**, 91 (1993); **B427**, 291 (1994).
[7] D. O'Connor, C. R. Stephens, and F. Freire, Mod. Phys. Lett. A **8**, 1779 (1993).
[8] N. Tetradis and C. Wetterich, Nucl. Phys. **B398**, 659 (1993).
[9] B. Bergerhoff, F. Freire, D. F. Litim, S. Lola, and C. Wetterich, Phys. Rev. B **53**, 5734 (1996).
[10] B. Bergerhoff, D. F. Litim, S. Lola, and C. Wetterich, Int. J. Mod. Phys. A **11**, 4273 (1996).
[11] N. Tetradis and D. F. Litim, Nucl. Phys. **B464**, 492 (1996).
[12] N. Tetradis, Nucl. Phys. **B488**, 92 (1997).
[13] D. F. Litim, Phys. Lett. B **393**, 103 (1997).
[14] W. Buchmüller, T. Helbig, and D. Waliser, Nucl. Phys. **B407**, 387 (1993).
[15] A. Hebecker, Z. Phys. C **60**, 271 (1993).
[16] W. Buchmüller, Z. Fodor, and A. Hebecker, Nucl. Phys. **B447**, 317 (1995).
[17] P. Dimopoulos, K. Farakos, and G. Koutsoumbas, Eur. Phys. J. C **1**, 711 (1998).
[18] K. Kajantie, M. Karjalainen, M. Laine, and J. Peisa, Phys. Rev. B **57**, 3011 (1998); Nucl. Phys. **B520**, 345 (1998).
[19] U. Ellwanger, Phys. Lett. B **335**, 364 (1994).
[20] F. Freire and C. Wetterich, Phys. Lett. B **380**, 337 (1996).
[21] D. F. Litim and J. M. Pawlowski, Phys. Lett. B **435**, 181 (1998); Nucl. Phys. B (Proc. Suppl.) **74**, 329 (1999); **74**, 325 (1999).
[22] D. F. Litim and J. M. Pawlowski, ''On Gauge Invariant Wilsonian Flows,'' hep-th/9901063.
[23] T. Morris, Phys. Lett. B **329**, 241 (1994).
[24] D. F. Litim, ''Wilsonian Flow Equations and Thermal Field Theory,'' hep-ph/9811272.
[25] M. d'Attanasio and M. Pietroni, Nucl. Phys. **B498**, 443 (1997).
[26] K. Kajantie, M. Laine, K. Rummukainen, and M. Shaposhnikov, Nucl. Phys. **B458**, 90 (1996).
[27] D. F. Litim, C. Wetterich, and N. Tetradis, Mod. Phys. Lett. A **12**, 2287 (1997).
[28] S. Coleman and E. Weinberg, Phys. Rev. D **7**, 1888 (1973).
[29] N. Tetradis and C. Wetterich, Nucl. Phys. **B383**, 197 (1992).
[30] K. Farakos, K. Kajantie, K. Rummukainen, and M. Shaposhnikov, Nucl. Phys. **B425**, 67 (1994).
[31] A. Strumia and N. Tetradis, Nucl. Phys. **B554**, 697 (1999).
[32] P. Arnold and L. Yaffe, Phys. Rev. D **49**, 3003 (1994).
[33] P. Arnold and D. Wright, Phys. Rev. D **55**, 6274 (1997).
[34] D. F. Litim, Phys. Lett. B **486**, 92 (2000); hep-th/0103195.